

---

# Circuits of Round-a-Face Quantum Channels

An Extension of the DUIRF Model

---

## Bachelor Thesis

MAX PLANCK INSTITUTE OF QUANTUM OPTICS

FACULTY OF PHYSICS  
AT THE LUDWIG MAXIMILIAN UNIVERSITY  
OF MUNICH

SUBMITTED BY

**Matthias Pawlik**

FIRST SUPERVISOR: DR. GEORGIOS STYLIARIS (MPQ)

SECOND SUPERVISOR: PROF. DR. IGNACIO CIRAC (MPQ)

THIRD SUPERVISOR: PROF. DR. JAN VON DELFT (LMU)

MUNICH, THE 1ST OF FEBRUARY 2024



---

# Schaltungen aus Round-a-Face Quantenkanälen

Eine Erweiterung des DUIRF Modells

---

## Bachelorarbeit

MAX-PLANCK-INSTITUT FÜR QUANTENOPTIK  
FAKULTÄT FÜR PHYSIK  
AN DER LUDWIG-MAXIMILIANS-UNIVERSITÄT  
MÜNCHEN

VORGELEGT VON  
**Matthias Pawlik**

ERSTBETREUER: DR. GEORGIOS STYLIARIS (MPQ)  
ZWEITBETREUER: PROF. DR. IGNACIO CIRAC (MPQ)  
DRITTBETREUER: PROF. DR. JAN VON DELFT (LMU)

MÜNCHEN, DEN 01. FEBRUAR 2024



---

## Abstract

---

In this thesis, the exactly solvable DUIRF model of dual-unitary quantum circuits is generalised to noisy dynamics. When replacing conventional IRF gates with local quantum channels, we impose that solvability properties are preserved in circuits of this new class of *IRF channels*. This gives rise to several unitality constraints which allow to reduce the number of independent parameters in the matrix representation of the channel. We then explicitly parameterise an interesting subset of IRF channels which cannot be represented in the DUIRF framework and which goes beyond convex combinations of dual-unitary gates. Furthermore, we elaborate on the specific structure of these quantum channels that appear to be in one-to-one correspondence to constructions of CNOT gates. Besides that, we conclude that both the Completely Depolarising and Dephasing Channel are incompatible with the solvability constraints.



---

# Contents

---

<b>Abstract</b>	<b>iii</b>
<b>1 Introduction</b>	<b>1</b>
1.1 Motivation . . . . .	1
1.2 Tensor Network Notation . . . . .	2
<b>2 Fundamental Concepts of Quantum Information</b>	<b>5</b>
2.1 Notions of Quantum Channels . . . . .	5
2.1.1 Completely Positive Trace-Preserving Maps . . . . .	5
2.1.2 The Kraus Representation Theorem . . . . .	6
2.1.3 The Stinespring Dilation Theorem . . . . .	9
2.1.4 The Choi–Jamiołkowski Isomorphism . . . . .	10
2.2 Aspects of Quantum Circuits . . . . .	10
2.2.1 Multipartite Tensor Network States . . . . .	11
2.2.2 Quantum Circuit Theory . . . . .	13
2.2.3 Solvability of Quantum Circuits . . . . .	13
<b>3 Dual Unitary Interaction Round-a-Face Circuits</b>	<b>17</b>
3.1 Principles of the DUIRF Model . . . . .	17
3.1.1 Circuits of IRF Quantum Gates . . . . .	17
3.1.2 Complete Parametrisation of DUIRF Gates . . . . .	20
3.2 Solvability of DUIRF Circuits . . . . .	21
3.2.1 Spatio-temporal Correlation Functions . . . . .	21
3.2.2 Spatial Correlation Functions after Quantum Quenches . . . . .	23
<b>4 Extension of the IRF Model to Quantum Channels</b>	<b>27</b>
4.1 The Class of IRF Channels . . . . .	27
4.2 The Minimal Example . . . . .	29
4.3 Solvability of IRF Channel Circuits . . . . .	36
<b>5 Conclusion and Outlook</b>	<b>39</b>

<b>A Explanatory Notes and Computations</b>	<b>41</b>
A.1 The Relative State Method . . . . .	41
A.2 Purification of Quantum States . . . . .	42
A.3 Computations of the Minimal Example . . . . .	43
<b>Bibliography</b>	<b>47</b>
<b>Acknowledgement</b>	<b>51</b>



## Introduction

---

### 1.1 Motivation

We are nowadays witnessing a second quantum revolution giving rise to many new technologies and applications of quantum mechanics. It is of main interest to study the behaviour of quantum many-body systems that serve as processors in the thriving field of quantum computation. In this work, we are going to apply the methods of quantum information which allow to examine the physical evolution of such quantum systems. Given a quantum state, one typically visualises manipulations on this system with a network of quantum gates, also referred to as the quantum circuit. However, in many physically relevant setups, the complexity of the latter does not allow to perform time and memory efficient computations on it such that special constraints have to be imposed on the constituent quantum gates. The so-called dual-unitary quantum circuits are prominent classes of exactly solvable models in one spatial dimension that guarantee such efficiency property.

Nonetheless, dual-unitary dynamics does not directly apply to real-world systems because these are always subject to quantum noise. Therefore, in [KS23], the dual-unitary model has been generalised by substituting dual-unitary gates for local quantum channels. This is a promising approach since exact solutions within this framework already include noisy dynamics. In the same work, they derive solvability conditions on these circuits of quantum channels and outline how correlation functions may then be computed systematically.

Lately, Tomaž Prosen introduced another class of quantum gates in [Pro21] that also possesses a dual-unitarity property but exhibits a different gate structure. In contrast to conventional models, these newly proposed *Dual-Unitary Interaction Round-a-Face* (DUIRF) quantum gates locally act over three and not only two qudits. It has been shown in [CLV23] that there exists a collective representation of any type of dual-unitary gate in the Shaded Calculus formalism.

In this thesis, we aim to extend the notion of IRF gates to quantum channels, which we will refer to as IRF *channels*. This generalisation embeds them in the family of exactly solvable models of noisy quantum circuits that are highly valuable in the Noisy Intermediate-Scale Quantum (NISQ) era. In chapter §2, a range of fundamental concepts of quantum information will be presented. In particular, we will review the notion of a quantum channel from different physical perspectives. In a second step, we illustrate solvability issues that occur when contracting generic quantum circuits. Chapter §3 presents the principles of the DUIRF model and provides examples of calculations of two types of correlation functions. In chapter §4, we then characterise the class of IRF quantum channels and explicitly parameterise a subset of IRF-channels which preserves solvability and goes beyond convex combinations of DUIRF quantum gates. Eventually, the results of this work are reviewed in the conclusion §5. Some technical computations are outsourced to the appendix A.

## 1.2 Tensor Network Notation

This preface provides a dictionary of notations and conventions applied throughout the thesis. In the following, we introduce *Tensor Network Notation* (TNN) which is a convenient diagrammatic visualisation of tensor manipulations<sup>[1]</sup>. According to [BC17] one can view this graphical notation as a generalisation of the Einstein summation convention that allows to keep track of particularly large numbers of indices in complex computations.

Hereafter, we summarise some fundamental identities that will be essential for the understanding of many statements in the main chapters of this work. In TNN, boxes represent rank- $r$  tensors whose indices, denoted with little legs, may be grouped into inputs and outputs. By fixing the value of each index of the tensor, we are left with a single complex number. Hence, for  $k + k' = r$ , we may identify

$$\begin{array}{c}
 i'_1 \quad i'_{k'} \\
 | \quad | \\
 \dots \\
 | \quad | \\
 \boxed{R} \\
 | \quad | \\
 \dots \\
 | \quad | \\
 i_1 \quad i_k
 \end{array}
 \equiv
 (R)_{i_1, \dots, i_k}^{i'_1, \dots, i'_{k'}} \in \mathbb{C}^{d_1 \times \dots \times d_k \times d'_1 \times \dots \times d'_{k'}}$$

Figure 1.1: Rank- $r$  tensor in TNN with input indices  $i_1, \dots, i_k$  and output indices  $i'_1, \dots, i'_{k'}$

<sup>[1]</sup> Tensor Network Notation was first proposed by Roger Penrose in 1971 and applies to various fields of physics ranging from quantum field theory and general relativity to quantum information theory [BC17].

The binary tensor product is defined elementwise as  $[R \otimes R']_{i_1, \dots, i_k, j_1, \dots, j_l}^{i'_1, \dots, i'_{k'}, j'_1, \dots, j'_l} = (R)_{i_1, \dots, i_k}^{i'_1, \dots, i'_{k'}} \cdot (R')_{j_1, \dots, j_l}^{j'_1, \dots, j'_l}$  which graphically corresponds to merging two boxes:

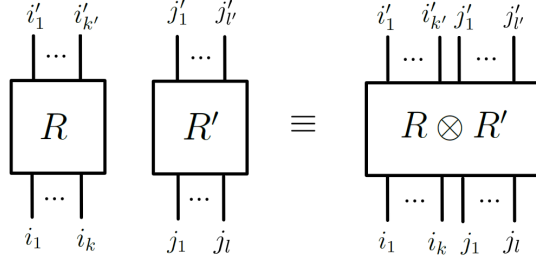


Figure 1.2: Binary tensor product of the tensors R and R' in TNN

If the  $x^{th}$  and  $y^{th}$  index of a tensor have identical dimension, one can perform the partial trace  $(tr_{x,y} R)_{i_1, \dots, i_x, \dots, i_k}^{i'_1, \dots, i'_y, \dots, i'_{k'}} = \sum_{\alpha=1}^{d_x} (R)_{i_1, \dots, \alpha, \dots, i_k}^{i'_1, \dots, \alpha, \dots, i'_{k'}}$  that can be represented by connecting the two legs which are summed over:

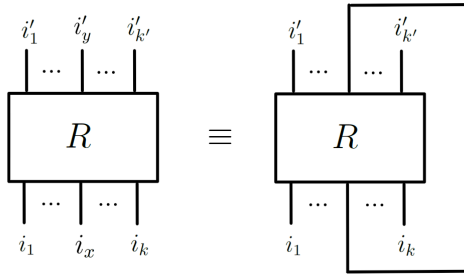


Figure 1.3: Partial trace over the indices  $i_x$  and  $i'_y$  of a tensor in TNN

Indices may be grouped and split freely taking advantage of row- or column-major ordering methods. For any bipartition of  $k$  and  $k'$  indices there exists a bijection of tensor elements to elements of an ordinary matrix of suitable dimensionality, referred to as the bisection of the tensor along this bipartition. For instance, the grouping of input and output indices to  $(R)_I^{I'} \in \mathbb{C}^{(d_1 \dots d_k) \times (d'_1 \dots d'_{k'})}$  with  $I = i_1 + d_1 \cdot i_2 + d_1 d_2 \cdot i_3 + \dots + d_1 \dots d_{k-1} \cdot i_k$  and  $I' = i'_1 + d'_1 \cdot i'_2 + d'_1 d'_2 \cdot i'_3 + \dots + d'_1 \dots d'_{k'-1} \cdot i'_{k'}$  yields the following graphical representation:

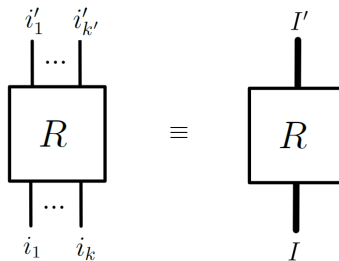


Figure 1.4: Grouping of the input and output indices of a tensor in TNN

Since any higher dimensional tensor may henceforth be thought of as a matrix, one can also find a singular value decomposition (SVD) with respect to this bisection  $(R)_{i_1, \dots, i_k}^{i'_1, \dots, i'_{k'}} = \sum_{\alpha} (U)_{\alpha}^{i'_1, \dots, i'_{k'}} \cdot$

$(S)_\alpha^\alpha \cdot (V^\dagger)_{i_1, \dots, i_k}^\alpha$  where  $U$  and  $V$  denote isometries ( $V^\dagger V = U^\dagger U = \mathbb{1}$ ) and  $S$  a diagonal matrix. In TNN this corresponds to

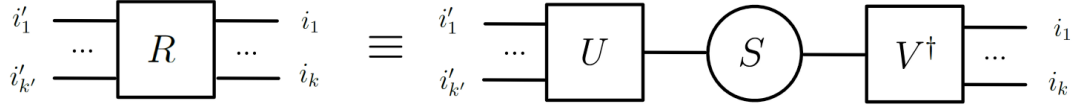


Figure 1.5: Singular value decomposition of a tensor in TNN

Tensor networks are now composed of several tensors connected by legs that indicate summations over the common indices. The dimensionality of the global tensor can be evaluated by multiplying the dimensions of all free legs. However, the difficulty of computing its value for fixed indices might strongly depend on the structure of the network. It is therefore of interest to find techniques to reduce the complexity of the global tensor, such as by imposing conditions on its constituents, for time and memory efficient contractions. In the context of this work, we want to consider ensembles of finite dimensional  $d$ -level quantum systems associated with Hilbert spaces  $\mathcal{H} \cong \mathbb{C}^d$ . Pure states may be depicted as boxes with a single leg whereas the illustration of mixed states in terms of density matrices necessarily requires both an input and output leg. The action of quantum mechanical operators on quantum states is then realized by simple contractions of the respective boxes.

## Fundamental Concepts of Quantum Information

---

This chapter provides an introduction to the fundamental principles of quantum information which are relevant for this work. We assume that the state of a quantum system is completely characterized by its density operator  $\rho$  which per definition needs to satisfy the conditions

(i)  $\rho \geq 0$                       **Positive Semi-Definiteness**

(ii)  $\text{tr}(\rho) = 1$                       **Normalisation**

Note that hermiticity  $\rho^\dagger = \rho$  is implicitly included in the first definition. From this postulate, we develop ways to transmit quantum information through quantum channels as presented in chapter §2.1. In a second step, we illustrate computational aspects in order to understand solvability issues of large quantum circuits. This should motivate the relevance of dual-unitary models which are worked with from chapter §3.1 on.

### 2.1 Notions of Quantum Channels

Having defined the properties of quantum states, we are interested in the propagation of quantum information over time. Such mappings between valid quantum states are referred to as *quantum channels*. There exist several equivalent representations of the latter originating from different physical perspectives on the quantum system. Hereinafter, we will discuss the most important ones and link them to each other.

#### 2.1.1 Completely Positive Trace-Preserving Maps

We first exhibit the most axiomatic approach. According to [CLT22] a *quantum channel*  $\varepsilon$  is defined as a completely positive trace preserving map (CPTM) between quantum states

$\rho \xrightarrow{CPT} \varepsilon(\rho) \equiv \rho'$  where one may identify  $\rho' \equiv \rho(t)$  as the time evolved quantum state. If the density operator  $\rho$  acts on a Hilbert space  $\mathcal{H}$ , we may consider arbitrary extensions  $\mathcal{H} \otimes \mathcal{H}_{ext}$ . Quantum channels are then defined as mappings satisfying the following conditions:

$$(iii) \quad (\varepsilon \otimes \mathbb{1}_d)(\tilde{\rho}) \geq 0 \quad \forall d = \dim(\mathcal{H}_{ext}) \quad \textbf{Complete Positivity}$$

$$(iv) \quad \text{tr}(\rho') = \text{tr}(\rho) \quad \textbf{Trace Preservation}$$

where  $\tilde{\rho} \in \mathcal{H} \otimes \mathcal{H}_{ext}$ . It is also customary to assume that  $\varepsilon$  is a linear map such that it respects convex mixtures of inputs. If we associate a quantum state to the environment living in  $\mathcal{H}_{ext}$  and coupled with our quantum state  $\rho$ , complete positivity ensures that the composite state evolves physically under all circumstances. Since experimentally one can never fully isolate a quantum system, this condition allows to examine such general open quantum systems. Trace preservation however mathematically guarantees the conservation of probabilities.

### 2.1.2 The Kraus Representation Theorem

For any quantum channel there can equivalently be found an explicit representation in terms of Kraus operators as derived in this theorem. Following [Pre98] and [Sch96], let us again consider the composite Hilbert space  $\mathcal{H} \otimes \mathcal{H}_{ext}$  of a system with its environment. For the proof we will apply the *Relative State Method* which is shortly described in the appendix A.1.

In a first step, we evaluate the image of a maximally entangled state  $\tilde{\rho} = |\Psi\rangle\langle\Psi|$  in the composite system under the action of  $\varepsilon \otimes \mathbb{1}_{ext}$  expressed as an ensemble of pure states

$$(\varepsilon \otimes \mathbb{1}_{ext})(|\Psi\rangle\langle\Psi|) = \sum_k q_k |\Phi\rangle_k \langle\Phi|_k \quad (2.1)$$

where  $q_k > 0$  and  $\sum_k q_k = 1$ . Note that for completely positive  $\varepsilon$  the resulting quantum state will again be positive semi-definite. We now implement the relative state method using the notion of an index state  $|\phi\rangle_{int}$  and relative state  $|\phi^*\rangle_{ext}$  as presented in the appendix to show

$$\varepsilon(|\phi\rangle_{int} \langle\phi|_{int}) = {}_{ext} \langle\phi^*| (\varepsilon \otimes \mathbb{1}_{ext})(|\Psi\rangle\langle\Psi|) |\phi^*\rangle_{ext} = \sum_k q_k {}_{ext} \langle\phi^*|\Phi_k\rangle \langle\Phi_k|\phi^*\rangle_{ext} \quad (2.2)$$

Furthermore, we may identify the *Kraus-Operators*  $\mathcal{F}_k$  acting on  $\mathcal{H}$  defined by the action

$$\mathcal{F}_k : |\phi\rangle_{int} \mapsto \sqrt{q_k} {}_{ext} \langle\phi^*|\Phi_k\rangle \quad (2.3)$$

Since the index state and relative state are linked by an anti-linear mapping, all  $\mathcal{F}_k$  are linear.

This allows us to also consider arbitrary mixed states as inputs in (2.2). Therefore any quantum channel  $\varepsilon$  acting over  $\mathcal{H}$  can be expressed in the Kraus decomposition given by

$$\varepsilon(\rho) = \sum_k \mathcal{F}_k \rho \mathcal{F}_k^\dagger \quad \text{with} \quad \sum_k \mathcal{F}_k^\dagger \mathcal{F}_k = \mathbb{1} \quad \textbf{Kraus Representation} \quad (2.4)$$

where the second equation needs to hold for trace preservation. The number of Kraus operators needed to represent the quantum channel depends on the rank of the image (2.1) that is bounded by  $\dim(\mathcal{H})$ . Moreover, one should notice that this representation is not unique: Any unitary transformed set of Kraus operators  $\tilde{\mathcal{F}}_{k'} = \sum_k \mathcal{F}_k U_{kk'}$  gives rise to the same Kraus decomposition.

We can conversely recover an ensemble representation of the quantum channel from a given Kraus decomposition. Let us adopt the notation from A.1, that is we have orthonormal bases  $\{|\alpha_i\rangle_{int}\}_{i=1}^n$  and  $\{|\beta_i\rangle_{ext}\}_{i=1}^d$ . Then if we know the action on the basis of  $\mathcal{H}$  given by

$$\varepsilon(|\alpha_i\rangle_{int} \langle \alpha_j|_{int}) = \sum_k \mathcal{F}_k |\alpha_i\rangle_{int} \langle \alpha_j|_{int} \mathcal{F}_k^\dagger \quad (2.5)$$

we may consider the extended map on the maximally entangled state  $|\Psi\rangle$

$$(\varepsilon \otimes \mathbb{1}_{ext})(|\Psi\rangle \langle \Psi|) = \frac{1}{n} \sum_{i,j} (\mathcal{F}_k |\alpha_i\rangle_{int} \otimes |\beta_i\rangle_{ext}) ({}_{int} \langle \alpha_j| \mathcal{F}_k^\dagger \otimes \langle \beta_j|_{ext}) = \sum_k q_k |\Phi_k\rangle \langle \Phi_k| \quad (2.6)$$

such that one may retrieve  $\sqrt{q_k} |\Phi_k\rangle = \frac{1}{\sqrt{n}} \sum_i \mathcal{F}_k |\alpha_i\rangle_{int} \otimes |\beta_i\rangle_{ext}$ . In that context, it is illuminating to point out how to interpret the unitary degree of freedom which is induced by the Kraus operators. For that, we will have to introduce the purification of a quantum state, a concept which is discussed in the appendix A.2. Let us consider two Kraus representations  $\sqrt{q_k} |\Phi_k\rangle$  and  $\sqrt{p_{k'}} |\Phi'_{k'}\rangle$  of the same quantum channel and study their purification

$$|\Upsilon\rangle = \sum_k \sqrt{q_k} |\Phi_k\rangle \otimes |\gamma_k\rangle_{pur} \quad \text{and} \quad |\Upsilon'\rangle = \sum_{k'} \sqrt{p_{k'}} |\Phi'_{k'}\rangle \otimes |\delta_{k'}\rangle_{pur} \quad (2.7)$$

living in the same purification space  $\mathcal{H}_{pur}$  with  $\dim(\mathcal{H}_{pur}) = m$  and spanned by two different sets of orthonormal bases  $\{|\gamma_k\rangle_{pur}\}_{k=1}^m$  and  $\{|\delta_{k'}\rangle_{pur}\}_{k'=1}^m$ . The GHJW theorem in A.2 asserts that purifications of any such Kraus representations are related by a unitary transformation in the purifying system. It therefore follows that

$$|\Upsilon'\rangle = \sum_{k'} \sqrt{p_{k'}} |\Phi'_{k'}\rangle \otimes |\delta_{k'}\rangle_{pur} = \sum_k \sqrt{q_k} |\Phi_k\rangle \otimes U_{pur} |\gamma_k\rangle_{pur} = \sum_{k',k} \sqrt{q_k} |\Phi_k\rangle \otimes U_{kk'}^{pur} |\delta_{k'}\rangle_{pur} \quad (2.8)$$

where in the last step we used that there is a unitary transformation between the bases of the purification space. Hence  $\sqrt{p_{k'}} |\Phi'_{k'}\rangle = \sum_k \sqrt{q_k} |\Phi_k\rangle U_{kk'}^{pur}$  with unitary  $U_{kk'}^{pur} \equiv U_{kk'}$  from which

we conclude  $\tilde{\mathcal{F}}_{k'} = \sum_k \mathcal{F}_k U_{kk'}$ . In this regard, the unitary invariance of the Kraus operators is a natural consequence of the GHJW theorem.

In keeping with the preface, let us now present an intuitive way to visualise the Kraus decomposition with the help of TNN. We will especially operate in the *Folded Picture Representation* which is introduced in the setting of [KS23]. From this point of view, density matrices are vectorised in order to avoid redundant graphical notation. If  $\{|n\rangle\}$  constitutes a basis of  $\mathbb{C}^d$  which induces a basis  $\{|m\rangle\langle n|\}$  for  $\mathbb{C}^d \otimes \mathbb{C}^d$ , then we map  $|m\rangle\langle n| \xrightarrow{vec} |m\rangle \otimes |n\rangle$ . In other words, we bend input indices upwards if we read the pictures from bottom to top. Now note that (2.4) is equivalent to a superoperator acting on the density operator of the quantum system. Hence, we may write  $\sum_k \mathcal{F}_k(\cdot)\mathcal{F}_k^\dagger \xrightarrow{vec} \sum_k \mathcal{F}_k \otimes \mathcal{F}_k^*$  where the  $*$  operation arises from the partial transposition in the vectorisation process, changing inputs and outputs of the Kraus operators  $\mathcal{F}_k^\dagger$ . Superoperators  $\sum_k \mathcal{F}_k(\cdot)\mathcal{F}_k^\dagger$  have the gentle feature that the operators acting from both sides on the quantum state are related by a  $\dagger$  operation allowing to further compactify the vectorised notation into a folded picture with identical information:

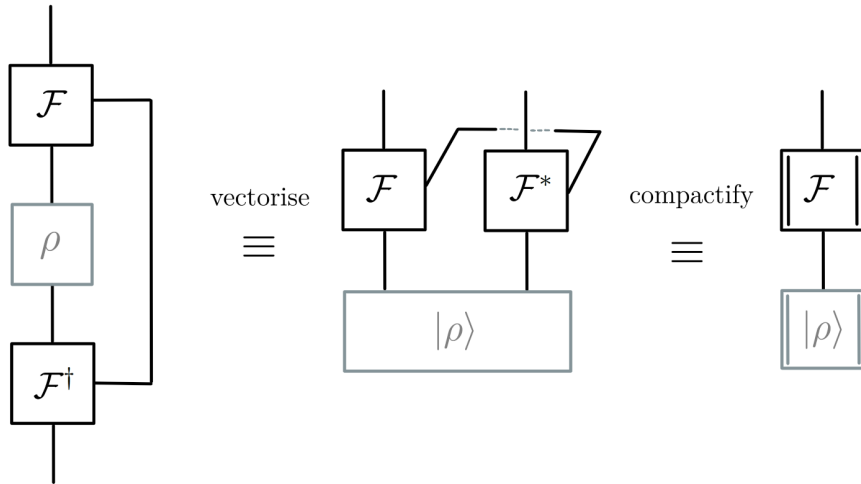


Figure 2.1: Kraus representation of a quantum channel in the folded picture

Note that in figure (2.1) we indicated the Kraus summation index with a closed wire between the Kraus operators which is graphically omitted in the folded picture. Quantum states that are acted on are indicated in gray colour and the timeline should henceforward be read from bottom to top in the vectorised notation. Moreover, we denote objects in the folded notation with double lines to stress that the quantum channel acts on a bipartition of indices of the vectorised state. This graphical method also extends to ensembles of qudits where one only needs to add the respective number of additional input and output legs to the initial state  $\rho$ . Lastly, let us elaborate on the special case of unitary dynamics. It is obvious to see that for



trivial Kraus indices the  $\sum_k$  disappears in formula (2.4). Then we rename  $\mathcal{F}_k \mapsto U$  such that

$$\varepsilon(\rho) = U\rho U^\dagger \quad \text{with} \quad U^\dagger U = \mathbb{1} \quad \textbf{Unitary Dynamics} \quad (2.9)$$

In graphical notation, one can recognise unitary dynamics directly by the omitted Kraus summation leg and by the blue colouring which will be applied throughout the whole thesis.

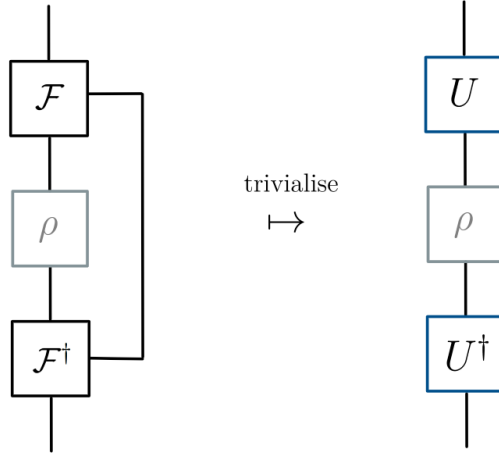


Figure 2.2: Trivial Kraus representation for unitary dynamics in the unfolded picture

### 2.1.3 The Stinespring Dilation Theorem

In the derivation of the Kraus representation, we treated the most general case of quantum channels to describe quantum systems coupled to an environment. However, if we also include the latter into our considerations, the overall dynamics of the closed quantum system will be unitary according to the postulates of quantum mechanics. The Kraus representation then naturally arises in the subsystem when tracing out the environment described by a quantum state  $|0\rangle$ . This so-called *Stinespring Dilation Theorem* can be understood in TNN [BC17]:

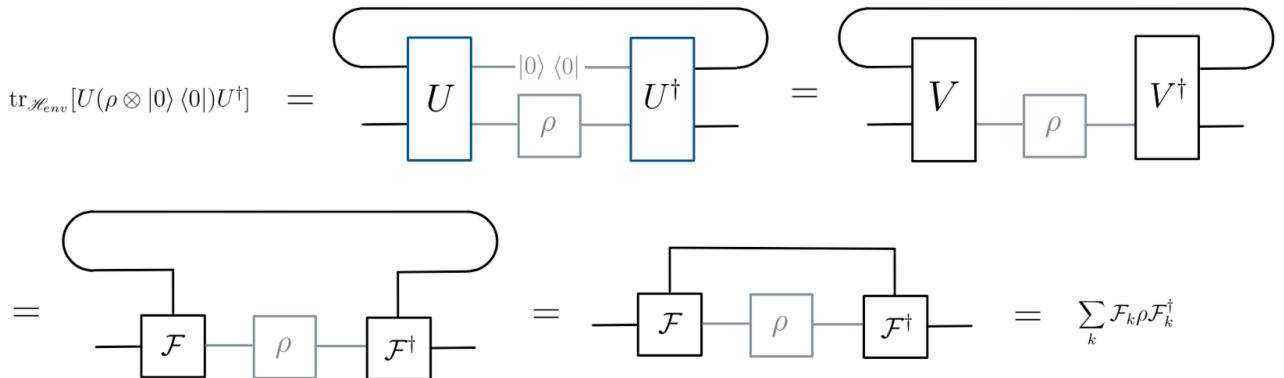


Figure 2.3: Graphical derivation of the Stinespring Dilation of a quantum channel

The unitary operator  $U$  only possesses three free indices if one keeps the environment state fixed. It can therefore be replaced by an isometry  $V$  (with  $V^\dagger V = \mathbb{1}$ ) which can be identified with the Kraus operators  $\mathcal{F}_k$ . One notices that unitary operators  $\tilde{U} = (\mathbb{1} \otimes U'_{env})U(\mathbb{1} \otimes U''_{env})$  generate the same quantum channel for some unitary  $U'_{env}$  and  $U''_{env}$  only acting on the environment [CLT22]. The assumption that the environment is in an initial product state is reasonable in many practical implementations [NC10]. Typically experimentalists reduce correlations between the system and the environment to a minimum before the experiment.

### 2.1.4 The Choi–Jamiołkowski Isomorphism

We have already worked with the Choi state of a quantum channel previously without explicitly mentioning it and examining its structure. If we consider the maximally entangled state  $|\Psi\rangle$  from chapter §2.1.2, then the *Choi state* is defined with respect to the quantum channel  $\varepsilon$  as

$$\sigma^\varepsilon = (\varepsilon \otimes \mathbb{1}_{ext})(|\Psi\rangle\langle\Psi|) \quad \text{with} \quad \text{tr}_{\mathcal{H}}(\sigma^\varepsilon) = \frac{\mathbb{1}_{ext}}{n} \quad \text{Choi state} \quad (2.10)$$

According to [CLT22], the *Choi–Jamiołkowski Isomorphism* describes a one-to-one-correspondence between any quantum channel  $\varepsilon$  and a Choi state  $\sigma^\varepsilon$ . This becomes apparent in the expression

$$n \text{tr}_{\mathcal{H}_{ext}}[\sigma^\varepsilon(\mathbb{1} \otimes \rho^T)] = n \text{tr}_{\mathcal{H}_{ext}}[(\varepsilon \otimes \mathbb{1}_{ext})(|\Psi\rangle\langle\Psi|)(\mathbb{1} \otimes \rho^T)] \quad (2.11)$$

$$= n \varepsilon \text{tr}_{\mathcal{H}_{ext}}[(|\Psi\rangle\langle\Psi|)(\mathbb{1} \otimes \rho^T)] \quad (2.12)$$

$$= n \varepsilon \text{tr}_{\mathcal{H}_{ext}}[(|\Psi\rangle\langle\Psi|)(\rho \otimes \mathbb{1}_{ext})] \quad (2.13)$$

$$= n \varepsilon(\rho) \text{tr}_{\mathcal{H}_{ext}}(|\Psi\rangle\langle\Psi|) \quad (2.14)$$

$$= \varepsilon(\rho) \quad (2.15)$$

where we used the identity  $(\mathbb{1} \otimes \rho^T)|\Psi\rangle = (\rho \otimes \mathbb{1}_{ext})|\Psi\rangle$ <sup>[1]</sup> and  $\dim(\mathcal{H}) = \dim(\mathcal{H}_{ext}) \equiv n$ .

By taking the partial trace with respect to  $\mathcal{H}_{ext}$  in (2.10) one may find the Kraus operators corresponding to that quantum channel as demonstrated in (2.2).

## 2.2 Aspects of Quantum Circuits

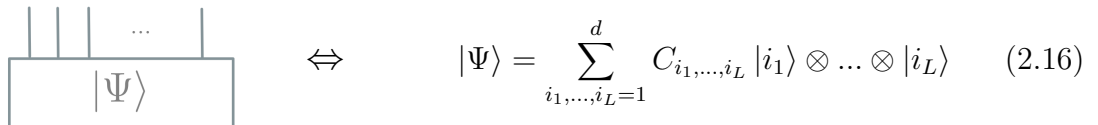
This section gives insights into computational aspects of tensor networks. Namely, we provide notions of quantum circuits and initial states which they might act on. Eventually, we illustrate the difficulty of efficiently contracting generic quantum circuits.

<sup>[1]</sup> This can readily be seen by expanding  $\rho = \sum_{i,j} \rho_{ij} |\alpha_i\rangle\langle\alpha_j|$  and inserting the definition of  $|\Psi\rangle$ .

### 2.2.1 Multipartite Tensor Network States

In the following we will derive an important class of initial states for one-dimensional quantum systems [BC17]. These so-called *Matrix Product States* (MPS) typically describe quantum low energy states of physically realistic systems efficiently. We now construct the TNN representation of such states step by step.

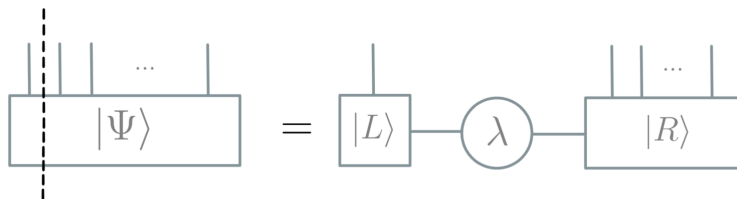
If one considers a one-dimensional system of  $L$  qudits with local Hilbert space dimension  $d$ , the most general ansatz for the quantum state of the composite system reads



$$|\Psi\rangle = \sum_{i_1, \dots, i_L=1}^d C_{i_1, \dots, i_L} |i_1\rangle \otimes \dots \otimes |i_L\rangle \quad (2.16)$$

Figure 2.4: Representation of a generic many-body quantum state in TNN

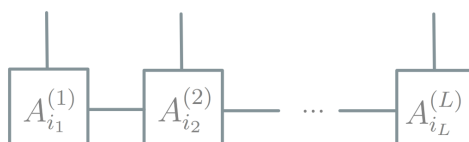
where all information on the quantum state is stored in the coefficients  $C_{i_1, \dots, i_L}$ . As the number of coefficients scales exponentially with  $d^L$ , one tries to find a simpler but still exact representation of the quantum state. In our case, the idea is to perform successive SVDs (as described in figure 1.5) to reduce the complexity of our state. At first, let us group the indices  $i_2$  to  $i_L$  which yields a SVD with respect to the first index  $i_1$ :



$$|\Psi\rangle = |L\rangle \otimes \lambda \otimes |R\rangle$$

Figure 2.5: First grouping step in the construction of MPS from successive SVDs

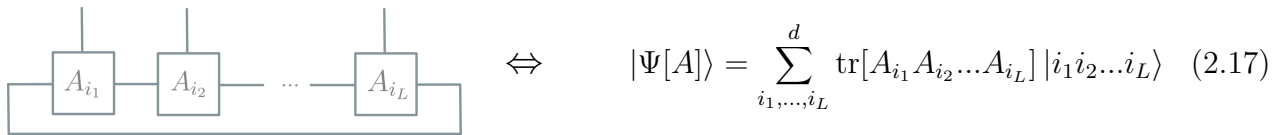
where the  $\{|L_i\rangle\}$  and  $\{|R_i\rangle\}$  are orthonormal sets of vectors. The remaining state physically corresponds to the Schmidt decomposition  $|\Psi\rangle = \sum_i \lambda_i |L_i\rangle \otimes |R_i\rangle$  with Schmidt coefficients  $\lambda_i$ . By repeating this procedure  $L-1$  times on the respective states  $|R_i\rangle$ , we are left with a decomposition into local tensors  $M^{(i)}$  and singular value tensors  $\lambda^{(i)}$ . Contracting the latter into the local tensors yields the generic form of a matrix product state:



$$A_{i_1}^{(1)} - A_{i_2}^{(2)} - \dots - A_{i_L}^{(L)}$$

Figure 2.6: Representation of a Matrix Product State in TNN

We note that by construction the MPS is not unique since we could have grouped the indices in any arbitrary order. The advantage of this representation comes into play if the number of non-zero singular values  $c$  in the matrices  $\lambda^{(i)}$  can be bounded by a *strong area law*<sup>[2]</sup>. In this case, we may truncate the zero Schmidt coefficients from the singular value tensors and remain with only  $\mathcal{O}(dLc^2)$  coefficients that exactly express the MPS. In figure (2.6) we call an uncontracted index a *physical index* whereas a *bond index* corresponds to the summation index between adjacent matrices  $A^{(i)}$ . Typically, one modifies the final form for convenience or to capture periodic states by connecting the tensors  $A_{i_1}^{(1)}$  and  $A_{i_L}^{(L)}$ . In case of translational invariance the MPS then writes



$$|\Psi[A]\rangle = \sum_{i_1, \dots, i_L} \text{tr}[A_{i_1} A_{i_2} \dots A_{i_L}] |i_1 i_2 \dots i_L\rangle \quad (2.17)$$

Figure 2.7: Matrix Product State with translational invariance in TNN

We are furthermore interested in treating ensembles of MPS that are realised by so-called *Matrix Product Density Operators* (MPDO). A mixed state  $\rho[A] = |\Psi[A]\rangle \langle \Psi[A]|$  may be expressed in the folded picture where we now also added further indices on the sides to allow for boundary conditions represented by tensors  $a_L$  and  $a_R$ :

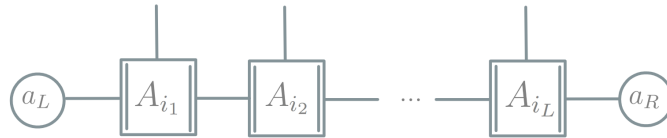
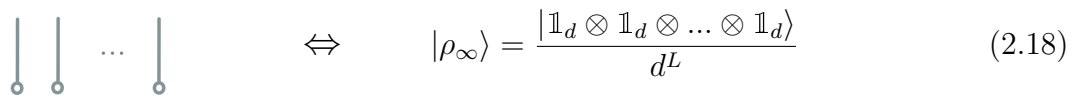


Figure 2.8: Matrix Product Density Operator in the folded picture

In chapter §3.2, we will engage with the so-called *infinite temperature*, or equivalently, *maximum entropy state* which is another type of multipartite TNN state. It can be viewed as the state of maximal disorder where thermal influence is overwhelming quantum coherence phenomena. It can be represented in the folded notation by a number of local vectorised identities that are symbolised by small circles [KS23].



$$|\rho_\infty\rangle = \frac{|\mathbb{1}_d \otimes \mathbb{1}_d \otimes \dots \otimes \mathbb{1}_d\rangle}{d^L} \quad (2.18)$$

Figure 2.9: Infinite temperature state of a quantum many-body system with  $L$  qudits

<sup>[2]</sup> Entanglement rank  $S_0 \leq \log c$  for some constant  $c$  where  $S_\alpha = \frac{1}{1-\alpha} \log \text{tr}(\rho^\alpha)$  denotes the  $\alpha$ -Rényi entropy.

### 2.2.2 Quantum Circuit Theory

Having prepared our system in an initial quantum state, we may simulate the physical evolution by acting quantum gates on them. In the case of closed quantum systems, the overall evolution has to be unitary. In fact, it can be shown that any unitary operation  $U$  acting over a Hilbert space  $\mathcal{H} = (\mathbb{C}^d)^{\otimes L}$  may be decomposed into a product of gates belonging to a small *universal set* of gates of which there exist many equivalent ones [Wan23]. Hence, we have to deal with a network of quantum gates, called *quantum circuit*, which reduces the task to the analysis of the constituent local unitary operations. Such qudit gates can themselves be reduced to and therefore be simulated by sequences of lower-dimensional qudit gates.

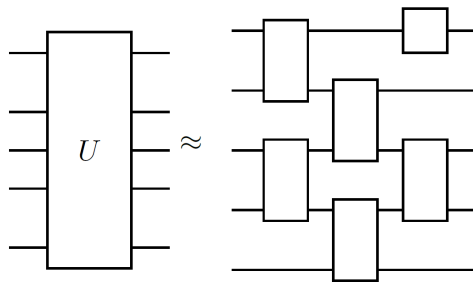


Figure 2.10: Reduction of a global unitary operation to locally acting unitary gates

In the scope of this work, we mainly engage with tripartite qudit gates introduced in chapter §3. It is also possible to construct circuits of quantum channels by switching into the folded picture representation. Such circuits then also capture the dynamics of open quantum systems whose dynamics do not need to be unitary in principal.

### 2.2.3 Solvability of Quantum Circuits

We ultimately provide an example that illustrates the computational difficulties when performing contractions of quantum circuits. This motivates the restriction to particular classes of quantum gates with gentle properties such that important physical computations may be carried out efficiently (see chapter §3.2).

Let us fix the free indices of the global tensor of an exemplary tensor network [BC17] and only denote summation indices in the graphical notation in figure (2.11). Since the computation of (2.19) does not depend on the order by which the constituent tensors  $R^{(j)}$  are contracted, there are several techniques with varying complexity and practicality to determine the value of the network. We give two examples of such contractions, also referred to as *bubbings*: In the first scenario (figure 2.12), we initially contract the tensors rightwards on top before returning from

$$\equiv \sum_{i_1, i_2, i_3, i_4, i_5, i_6, i_7} R_{i_1, i_3}^{(1)} R_{i_1, i_2, i_4}^{(2)} R_{i_2, i_5}^{(3)} R_{i_3, i_6}^{(4)} R_{i_4, i_6, i_7}^{(5)} R_{i_5, i_7}^{(6)} \quad (2.19)$$

Figure 2.11: Computation of quantum circuits

the left on the bottom. Here, the bubbling is marked in gray colour and the partially contracted tensor, which is kept in memory, in green colour.

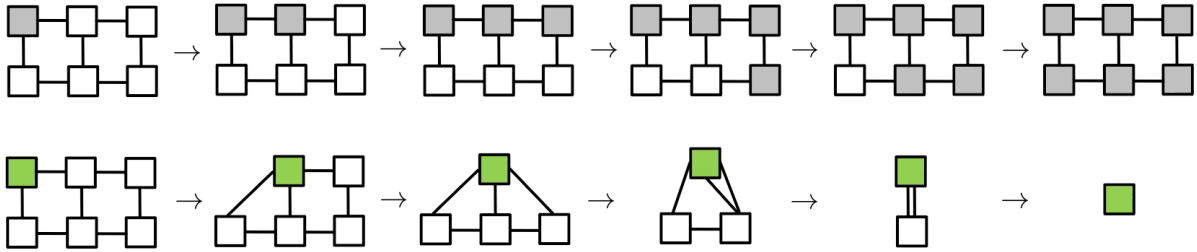


Figure 2.12: Inefficient bubbling of a tensor network (sample size  $L = 3$ )

This method works for small networks, however, for large ensembles of horizontal length  $L$ , the calculation becomes intractable. At the midpoint of the contraction the green tensor has rank  $L$  and therefore the number of entries scales with  $d^L$  when assuming bond dimension  $d$ . The required memory and run-time then also grow exponentially which renders the problem infeasible for large sizes. In contrast, by meandering from left to right, the rank of the green tensor never exceeds three such that the time and memory cost only scale linearly (figure 2.13).

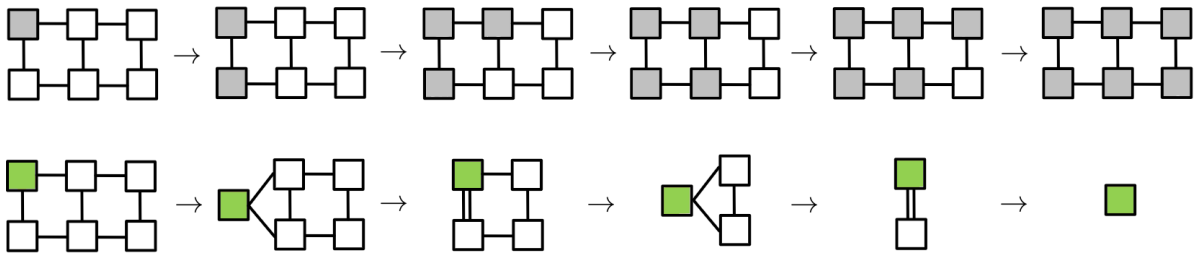


Figure 2.13: Efficient bubbling of a tensor network (sample size  $L = 3$ )

While in these examples there exist both efficient and inefficient bubblings, the graph structure of other tensor networks does generally not admit any efficient contraction ordering. For instance, one can mention the two-dimensional grid (figure 2.14). This example is of particular interest since it is closely related to our setup discussed in §3.1.1. It is clear to see that at any







---

## Dual Unitary Interaction Round-a-Face Circuits

---

### 3.1 Principles of the DUIRF Model

In this chapter we want to present an interesting class of quantum circuits recently proposed by Tomaz Prosen in [Pro21]. These so-called *Dual-Unitary Interaction Round-a-Face* circuits are composed of locally interacting quantum gates over three qudits of identical Hilbert space dimension  $d$ , hereafter referred to as DUIRF( $d$ ). One can comprehend this class as a subset of the unitary class  $\text{IRF}(d) \subset \text{DUIRF}(d)$  fulfilling an additional space-wise unitarity condition. Let us therefore introduce the structure of *Interaction Round-a-Face* (IRF-)circuits first and then deduce the implications imposed on them by this space-unitarity constraint.

#### 3.1.1 Circuits of IRF Quantum Gates

An element  $U_{\text{IRF}} \in \text{IRF}(d)$  is defined as the following tripartite quantum gate:

$$U_{\text{IRF}} = \sum_{i,j,k,j'=1}^d (u_{ik})_j^{j'} |i\rangle \otimes |j'\rangle \otimes |k\rangle \langle i| \otimes \langle j| \otimes \langle k| \quad (3.1)$$

where each element of the set  $\{u_{ik} \in U(d)\}_{i,k \in \{1, \dots, d\}}$  is unitary with respect to the input index  $j$  and output index  $j'$ . In the graphical notation, such quantum gates can be represented as 2-controlled 3-qudit gates or equivalently as compact faces:

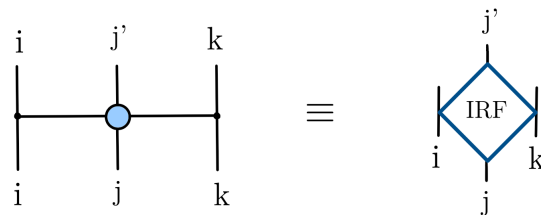


Figure 3.1: IRF-gate in controlled unitary gate and face representation

We consider the following setup: Let us align  $L \in \mathbb{N}$  qudits on sites  $x$  along one dimension assuming periodic boundary conditions  $x + L \equiv x$  for simplicity. Each qudit is living in a  $d$ -dimensional Hilbert space  $\mathcal{H}_1 = \mathbb{C}^d$  such that the  $d^L$ -dimensional composite system reads  $\mathcal{H} = \mathcal{H}_1^{\otimes L}$ . One can arrange the IRF circuit by alternately applying the generators  $\mathcal{U}^e = \prod_{x=1}^L U_{2x-1,2x,2x+1}^{IRF}$  and  $\mathcal{U}^o = \prod_{x=1}^L U_{2x,2x+1,2x+2}^{IRF}$  where the gates  $U_{i,j,k}^{IRF}$  act on sites  $i, j$  and  $k$  respectively. The corresponding quantum circuit is depicted in both the conventional and the face notation:

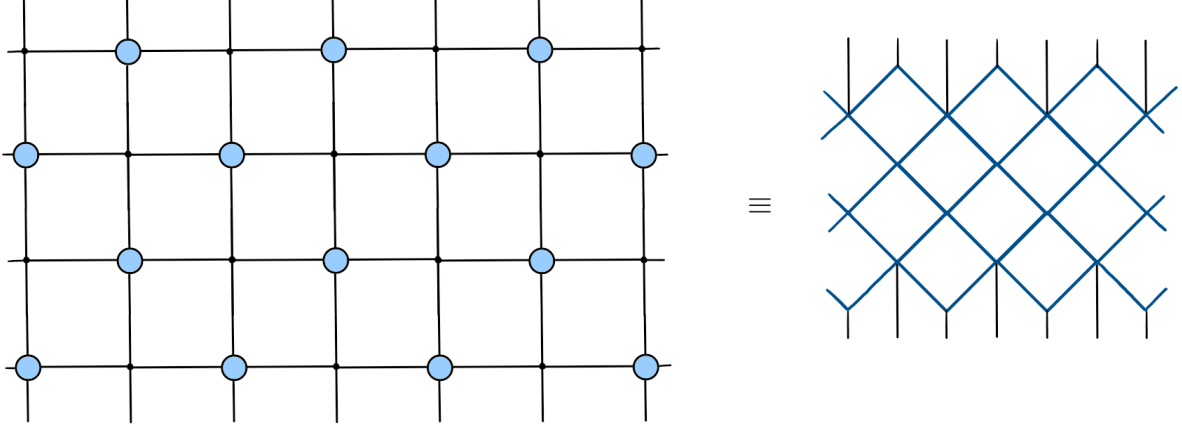


Figure 3.2: IRF-circuit in controlled unitary gate and face representation

One should also mention that gauge transformations  $U_{IRF} \mapsto (\Delta^\dagger \otimes g^\dagger \otimes \Delta^\dagger) U_{IRF} (\Delta \otimes g \otimes \Delta)$  with  $g \in SU(d)$  and  $\Delta_j^{j'} = \delta_{jj'} e^{i\theta_j}$  with  $\theta_j \in [0, 2\pi)$  yield identical quantum circuits, where one phase  $\theta_j$  may be fixed arbitrarily without loss of generality. The time unitarity condition  $U_{IRF}^\dagger U_{IRF} = \mathbb{1}$  may be written in graphical notation as follows

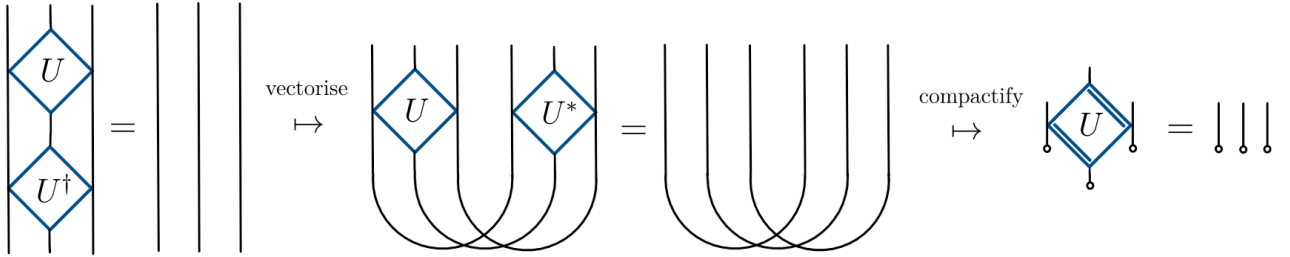


Figure 3.3: Time unitarity conditions of IRF-gates

where small circles indicate a partial trace along the summed over legs. If we explicitly write out this unitarity condition for IRF-gates mathematically, we obtain

$$\sum_{m=1}^d (u_{ik})_m^{j'} (u_{ik}^\dagger)_j^m = \delta_{jj'} \quad \forall i, k = 1, \dots, d \quad \text{Time Unitarity} \quad (3.2)$$

Since unitarity implies that the first identity in the figure (3.3) must also hold when reading it

in the other time direction from top to bottom, we get a further similar identity:

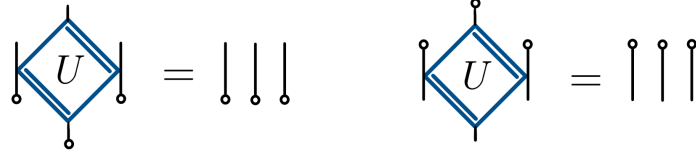


Figure 3.4: Time unitarity conditions of IRF-gates in the folded picture

By only swapping indices in the coefficients  $(u_{ik})_j^{j'} \mapsto (u_{jj'})_i^k$  of equation (3.1), let us now define the *dual gate*  $\tilde{U}_{IRF}$  of an IRF-gate in the following manner:

$$\tilde{U}_{IRF} = \sum_{i,j,k,j'=1}^d (u_{jj'})_i^k |i\rangle \otimes |j'\rangle \otimes |k\rangle \langle i| \otimes \langle j| \otimes \langle k| \quad (3.3)$$

which by renaming indices writes

$$= \sum_{i,j,k,j'=1}^d (u_{ik})_j^{j'} |j\rangle \otimes |k\rangle \otimes |j'\rangle \langle j| \otimes \langle i| \otimes \langle j'| \quad (3.4)$$

where one may identify  $(\tilde{u}_{jj'})_i^k := (u_{ik})_j^{j'}$ . This form suggests to interpret the IRF-gate space-wise with input index  $i$  and output index  $k$  which may be expressed in TNN as follows:

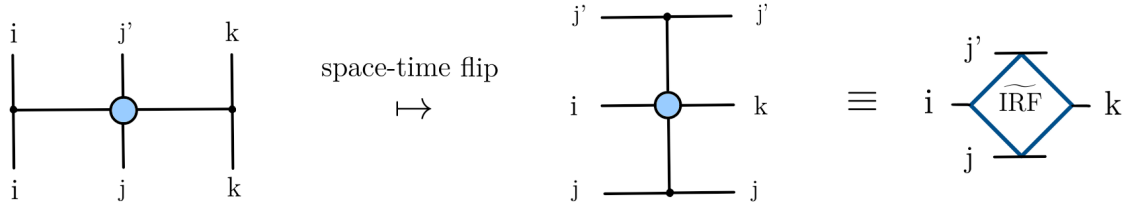


Figure 3.5: Dual IRF-gate in controlled gate and face representation

These dual gates may obey a space unitary condition  $\tilde{U}_{IRF}^\dagger \tilde{U}_{IRF} = \mathbb{1}$  in analogy to the notion of unitarity in the conventional time direction.

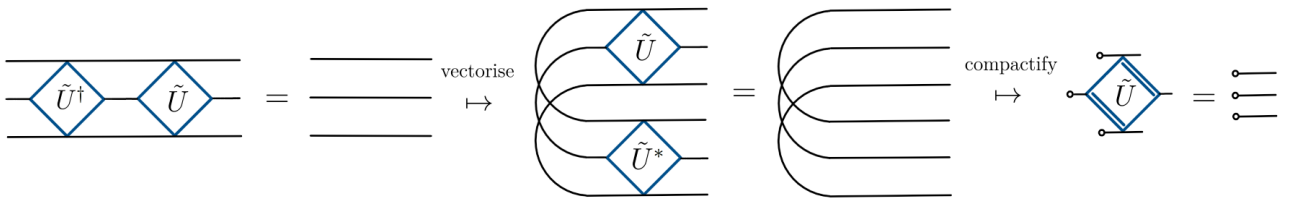


Figure 3.6: Space-wise unitarity condition of dual IRF-gate

Such condition mathematically translates to

$$\sum_{m=1}^d (\tilde{u}_{jj'})_m^k (\tilde{u}_{jj'}^\dagger)_i^m = \delta_{ik} \quad \forall j, j' = 1, \dots, d \quad \text{Space Unitarity} \quad (3.5)$$

Similarly, when interpreting along the other space direction, one may find the second space unitarity condition. Hence, we conclude



Figure 3.7: Space unitarity conditions of Dual IRF-gates in the folded picture

An element  $U_{DUIRF} \in \text{DUIRF}(d)$  is an IRF-gate fulfilling the time unitarity conditions (3.4) and whose dual gate also satisfies the space unitarity conditions (3.7). In order to stress that additional property, dual-unitary dynamics will henceforth be represented in purple colours.

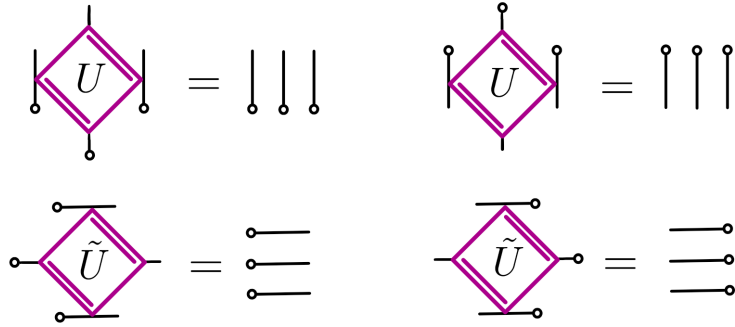


Figure 3.8: Unitarity conditions of the DUIRF-gate in the folded picture

### 3.1.2 Complete Parametrisation of DUIRF Gates

We now want to review [Pro21] where a complete parametrisation of the  $\text{DUIRF}(2)$  class was elaborated. In the same manner, in chapter §4.1 we will parameterise a subset of the generalised IRF channels. In both cases let us focus on qubits ( $d = 2$ ): An element of the unitary group  $U(2)$  may be represented in terms of Euler angles as a matrix

$$u_{ik} = e^{i\phi_{ik}} \begin{pmatrix} e^{i\nu_{ik}} \cos \theta_{ik} & e^{i\eta_{ik}} \sin \theta_{ik} \\ -e^{-i\eta_{ik}} \sin \theta_{ik} & e^{-i\nu_{ik}} \cos \theta_{ik} \end{pmatrix} \quad (3.6)$$

with  $\phi_{ik}, \nu_{ik}, \eta_{ik}, \theta_{ik} \in [0, 2\pi)$  where  $i, k = 1, 2$ . Thus by only considering the time unitarity condition we are left with 16 real parameters in total. Let us now add the space unitarity constraint imposed by the dual:  $\sum_{m=1}^d (\tilde{u}_{jj'})_m^k (\tilde{u}_{jj'}^\dagger)_i^m = \sum_{m=1}^d (u_{mk})_j^{j'} (u_{mi}^*)_j^{j'} = \delta_{ik} \forall j, j' = 1, 2$  which results in a set of equations for the angles  $\theta_{ik}$ :

$$\cos^2 \theta_{11} = \sin^2 \theta_{12}, \quad \cos^2 \theta_{22} = \sin^2 \theta_{21} \quad (3.7)$$

$$\cos \theta_{11} \cos \theta_{12} + \cos \theta_{21} \cos \theta_{22} = 0 \quad (3.8)$$

$$\sin \theta_{11} \sin \theta_{12} + \sin \theta_{21} \sin \theta_{22} = 0 \quad (3.9)$$

as well as a set of linear equations for the other angles given by

$$\nu_{22} = \nu_{12} + \nu_{21} - \nu_{11} \quad (3.10)$$

$$\eta_{22} = \eta_{12} + \eta_{21} - \eta_{11} \quad (3.11)$$

$$\phi_{22} = \phi_{12} + \phi_{21} - \phi_{11} \quad (3.12)$$

We may then also express all the angles in the first set of equations through  $\theta_{22}$ :

$$\theta_{11} = \theta_{22} + \pi, \quad \theta_{12} = \theta_{21} = \theta_{22} + \frac{\pi}{2} \quad (3.13)$$

As we have 10 free independent parameters  $\{\theta_{22}, \nu_{11}, \nu_{12}, \nu_{21}, \eta_{11}, \eta_{12}, \eta_{21}, \phi_{11}, \phi_{12}, \phi_{21}\}$ , we assign the dimension  $\dim \text{DUIRF}(2) = 10$  to this class of gates. If one recalls the gauge invariance group of IRF-gates  $SU(2) \otimes U(1)^{\otimes(2-1)}$  with 4 free parameters and one includes an overall phase, we are effectively left with a 5-parametric set of physically not equivalent DUIRF-gates.

## 3.2 Solvability of DUIRF Circuits

In this chapter, we will give evidence of the advantages when dealing with correlation functions within the DUIRF framework. Beginning with the computation of spatio-temporal correlation functions, we then also analyse spatial correlation functions after quantum quenches.

### 3.2.1 Spatio-temporal Correlation Functions

Let us first return to the space-time lattice illustrated in (3.2). An important physical problem is the computation of *space-time correlation functions* of local observables in the tracial, infinite temperature state, which was introduced in §2.2.1. These are of fundamental interest in many areas of condensed matter and statistical physics [Pro21]. For a pair of two-site, traceless<sup>[1]</sup> observables  $a_x$  and  $b_y$  acting on sites  $(x, x + 1)$  and  $(y, y + 1)$  respectively, one defines the correlation function

$$f_{a,b}(x, y; t) = \lim_{L \rightarrow \infty} \frac{1}{\dim \mathcal{H}} \text{tr}(a_x U^t b_y U^{-t}) \quad (3.14)$$

where  $U^t$  denotes the unitary operator evolving the quantum system until time  $t$ . We may again switch into the folded picture to further simplify this expression by defining  $W^t = U^t \otimes (U^t)^*$  and the vectorised operators (3.15), (3.16) and (3.17) where  $\dim \mathcal{H} = d$  is the local Hilbert space dimension.

---

<sup>[1]</sup> This simplification can always be done by redefining  $a \rightarrow a - \text{tr}(a)/\text{tr}(\mathbb{1})\mathbb{1}$  and similarly for  $b$ , as well as using the linearity of the correlation function [CLV23].

$$\|a\rangle = \frac{1}{d} \sum_{i,i'=1}^d \sum_{j,j'=1}^d a_{ij}^{i'j'} (|i'\rangle \otimes |i\rangle) \otimes (|j'\rangle \otimes |j\rangle) \quad (3.15)$$

$$\|b\rangle = \frac{1}{d} \sum_{i,i'=1}^d \sum_{j,j'=1}^d b_{ij}^{i'j'} (|i'\rangle \otimes |i\rangle) \otimes (|j'\rangle \otimes |j\rangle) \quad (3.16)$$

$$\|o\rangle = \frac{1}{\sqrt{d}} \sum_{i=1}^d |i\rangle \otimes |i\rangle \quad (3.17)$$

With  $\|a_x\rangle = \|o\rangle^{\otimes(x-1)} \otimes \|a\rangle \otimes \|o\rangle^{\otimes(L-x-1)}$  and  $\|b_y\rangle = \|o\rangle^{\otimes(y-1)} \otimes \|b\rangle \otimes \|o\rangle^{\otimes(L-y-1)}$ , equation (3.14) eventually reduces to the simpler form

$$f_{a,b}(x, y; t) = \lim_{L \rightarrow \infty} \langle b_y \| W^t \| a_x \rangle \quad (3.18)$$

which in TNN corresponds to the left side of figure (3.9). By applying the time unitarity condition (3.4), the quantum circuit can be simplified to the blue shaded faces which in general does not yet guarantee solvability. If we additionally assume space unitarity (3.7), the quantum circuit either vanishes or can be computed efficiently.

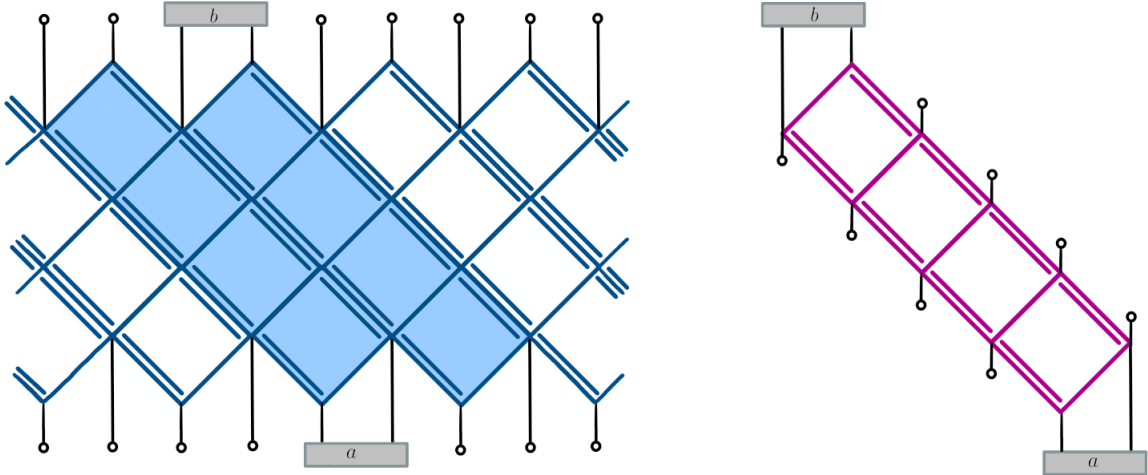
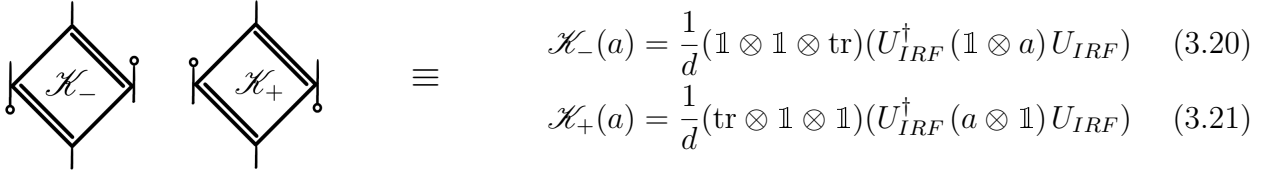


Figure 3.9: Computation of spatio-temporal correlation functions in TNN

The computations suggest that only if the support of the operators  $a$  and  $b$  is shifted precisely by  $2t$ , as on the right side of figure (3.9), we have non vanishing correlation functions. The time steps are chosen such that a single application of one of the generators  $\mathcal{U}^{e,o}$  corresponds to  $\Delta t = 0.5$ . In case that we allow for dual unitarity on the left side of the upper figure, the simplifications include the contraction  $\langle o \| a \rangle = \langle b \| o \rangle = 0$  and therefore yield zero correlations. Also note that causal interaction between different sites may only happen within the two light cones originating from the local observables. One therefore says that the light-cone correlators are non-vanishing along the light rays. We may summarise our result with

$$f_{a,b}(x, y; t) = \delta_{y, x+2t} \delta_{\text{mod}(x,2),1} \text{tr}(b \mathcal{K}_+^{2t}(a)) + \delta_{y, x-2t} \delta_{\text{mod}(x,2),0} \text{tr}(b \mathcal{K}_-^{2t}(a)) \quad (3.19)$$

by expressing the correlators in terms of sequences of CPTMs over the two-site Hilbert space



$$\mathcal{K}_-(a) = \frac{1}{d}(\mathbb{1} \otimes \mathbb{1} \otimes \text{tr})(U_{IRF}^\dagger(\mathbb{1} \otimes a)U_{IRF}) \quad (3.20)$$

$$\mathcal{K}_+(a) = \frac{1}{d}(\text{tr} \otimes \mathbb{1} \otimes \mathbb{1})(U_{IRF}^\dagger(a \otimes \mathbb{1})U_{IRF}) \quad (3.21)$$

Figure 3.10: Correlation maps of the light cone correlators

The correlation maps  $\mathcal{K}_\pm$  have large trivial subspace and can still be reduced to a simpler form. Consider the rank-1 projector  $\mathcal{D}(|j\rangle\langle j'|) = \delta_{j,j'}|j\rangle\langle j'|$  and the invariance of the maps under

$$\mathcal{K}_-(\mathbb{1} \otimes \mathcal{D}) = (\mathcal{D} \otimes \mathbb{1})\mathcal{K}_- = \mathcal{K}_- \quad (3.22)$$

$$\mathcal{K}_+(\mathcal{D} \otimes \mathbb{1}) = (\mathbb{1} \otimes \mathcal{D})\mathcal{K}_+ = \mathcal{K}_+ \quad (3.23)$$

Let us then define the diagonally projected maps  $\mathcal{K}'_\pm = (\mathcal{D} \otimes \mathcal{D})\mathcal{K}_\pm(\mathcal{D} \otimes \mathcal{D})$ . Together with the projector property  $\mathcal{D}^2 = \mathcal{D}$  equations (3.22) and (3.23) imply for the diagonally projected sequence of correlation maps that  $(\mathcal{K}'_\pm)^t = (\mathcal{D} \otimes \mathcal{D})\mathcal{K}_\pm^t(\mathcal{D} \otimes \mathcal{D})$ . In the formula for  $f_{a,b}$  we can therefore substitute  $\text{tr}(b\mathcal{K}'_\pm^t(a)) = \text{tr}(b_d(\mathcal{K}'_\pm)^t(a_d))$  with  $a_d = \mathcal{D} \otimes \mathcal{D}a$  and  $b_d = \mathcal{D} \otimes \mathcal{D}b$ . One can further specify the matrix elements of the correlation maps in the computational basis to

$$(\mathcal{K}'_+)^{i'j'}_{ij} = \frac{1}{d} |(u_{ij'})^{i'}_j|^2 \quad \text{and} \quad (\mathcal{K}'_-)^{i'j'}_{ij} = \frac{1}{d} |(u_{i'j})^i_{j'}|^2 \quad (3.24)$$

revealing *bistochastic*<sup>[2]</sup> and even *dual bistochastic* matrices under space-time flipping [Pro21]<sup>[3]</sup>. Since the maps  $\mathcal{K}'_\pm$  annihilate operators acting trivially on only one site, the simplest non-trivial correlations are two-site observables. In summary, the decay of the correlation along the light ray is determined by the spectra of the matrices (3.24). The computation time of  $f_{a,b}$  only scales linearly with the size of the quantum circuit, hence we call this model exactly solvable.

### 3.2.2 Spatial Correlation Functions after Quantum Quenches

In close analogue to the computation of *spatial correlation functions* after a *quantum quench* in [KS23], we demonstrate how these can be computed efficiently for DUIRF quantum circuits. That is, we consider the spatial correlations of an initial density matrix which has evolved under some unitary operation:

$$g_{a,b}(x, y; t) = \lim_{L \rightarrow \infty} \langle a_x b_y || W^t || \rho(0) \rangle \quad (3.25)$$

<sup>[2]</sup> Square matrices  $x = (x)_{ij}$  whose columns and rows sum up to one:  $\sum_i x_{ij} = \sum_j x_{ij} = 1$ .

<sup>[3]</sup> In fact, one can also identify the maps  $\mathcal{K}'_\pm$  with classical *Markov chains* from probability theory.

Let us by  $W^t$  again denote a unitary operation in the folded picture and we further define the operator  $||a_x b_y\rangle = ||\circ\rangle^{\otimes(x-1)} \otimes ||a\rangle \otimes ||\circ\rangle^{\otimes(y-x)} \otimes ||b\rangle \otimes ||\circ\rangle^{\otimes(L-y-1)}$  which includes two two-site observables  $a_x$  and  $b_y$ . Other than in §3.2.1, we now contract with an initial state  $|\rho(0)\rangle$  which we will generally assume to be a translation-invariant MPDO as defined in §2.2.1. The computation of  $g_{a,b}$  graphically translates to the evaluation of

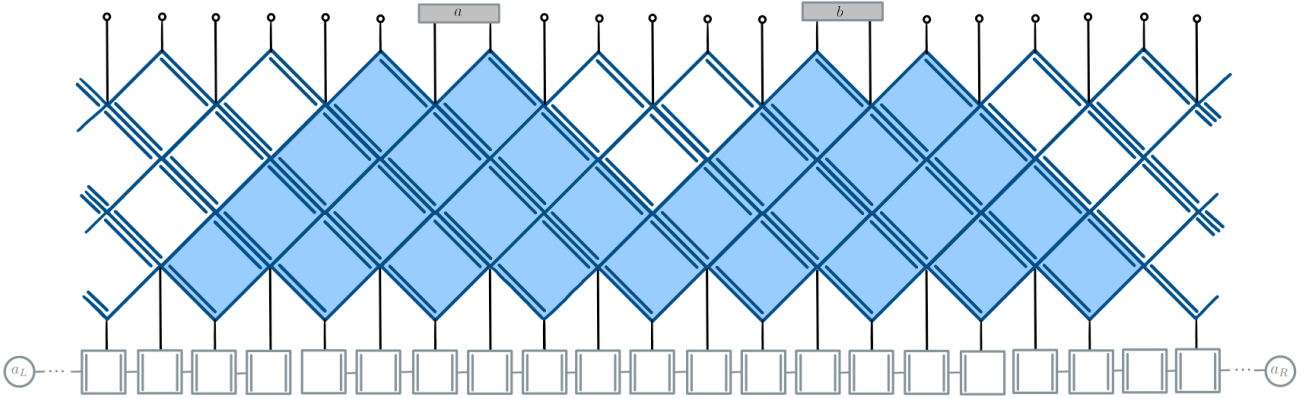


Figure 3.11: Computation of spatial correlation functions after a quantum quench

The MPDO is taken to be normalised in the thermodynamic limit  $L \rightarrow \infty$ , meaning that the

space transfer matrix  $E(0) = \begin{array}{c} \circ \\ \boxed{E(0)} \end{array}$  has to satisfy  $\lim_{L \rightarrow \infty} \text{tr} \rho(0) = \lim_{L \rightarrow \infty} \text{tr} E(0)^L = 1$ .

By only considering trace preservation, that is time unitarity in the backwards time direction, the computation reduces to the blue shaded faces. In order to guarantee solvability, we have to impose additional structure on the local matrices of the MPDO. It turns out that the characterisation of such solvable states for DUIRF circuits is highly non-trivial and requires a deeper analysis<sup>[4]</sup> which is outside the scope of this work. However, we provide solvability conditions for trivial boundary conditions. That is, we define

$$\begin{array}{c} \circ \\ \boxed{\phantom{E(0)}} \end{array} = \begin{array}{c} | \\ \circ \end{array} \quad \text{and} \quad \begin{array}{c} \boxed{\phantom{E(0)}} \\ \circ \end{array} = \begin{array}{c} \circ \\ | \end{array} \quad \text{with} \quad \begin{array}{c} \circ \\ \circ \end{array} = 1$$

Figure 3.12: Definition of solvability conditions

which corresponds to the infinite temperature state and reduces the circuit immediately to zero if the two-site observables are taken traceless. More generally one expects that for other classes of solvable initial states, the circuit further simplifies with the space unitarity condition to a quantum circuit that is generically of the following form:

<sup>[4]</sup> For conventional dual-unitary circuits such an analysis has been done in [KS23]. Furthermore, [Pro21] suggests that results on solvable initial states should have their analogues in the DUIRF model.



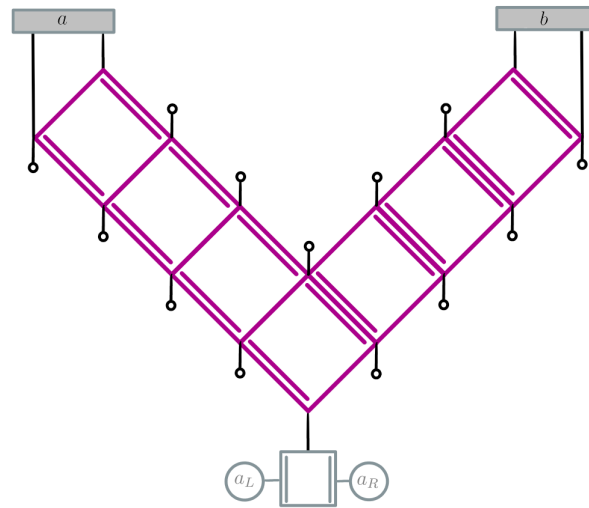


Figure 3.13: Reduced spatial correlation function after a quantum quench

and where boundary conditions come into play at the intersection of the two light rays. It remains an open question whether non-trivial solvable states require translational invariance over matrices with local support larger than one, which might still modify the concrete structure of the reduced state on the bottom of figure (3.13). Since in this scenario, correlations are non-zero if and only if the supports of the two-site observables are at the respective reflected positions of the light ray, the computational complexity is expected to scale linearly again. Hence, we have outlined two physical applications in the realm of closed quantum systems where the DUIRF model guarantees solvability. Chapter §4 shall now propose an extension of this model to noisy quantum circuits preserving solvability in the above mentioned sense.



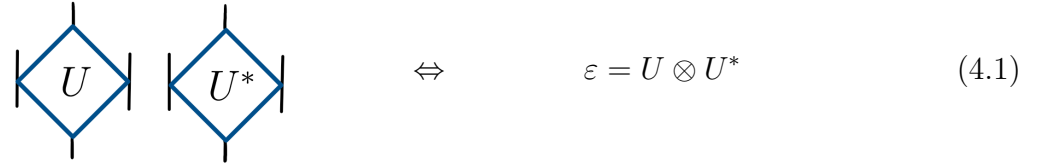
---

Extension of the IRF Model to Quantum Channels

---

### 4.1 The Class of IRF Channels

The key idea of this thesis is to embed the  $\text{IRF}(d)$  class in the formalism of quantum channels. We have seen in §2.1.2 that for unitary quantum gates the summation index disappears in the Kraus representation of the corresponding channel. Hence, for  $U \in \text{IRF}(d)$ , the quantum channel  $\varepsilon$  can be written in vectorised form as



$$\begin{array}{|c} \diagup \\ U \\ \diagdown \end{array} \begin{array}{|c} \diagdown \\ U^* \\ \diagup \end{array} \Leftrightarrow \varepsilon = U \otimes U^* \quad (4.1)$$

Figure 4.1: Representation of an IRF-gate in the vectorised picture

We may ask if there is an extension of the IRF class to quantum channels, including (dual-) unitary dynamics as a special case, such that global solvability features are preserved. We will investigate on solvability aspects in more detail in chapter §4.3. Henceforth, such generalisations of unitary IRF gates will be referred to as IRF *channels* that are elements of the  $\text{IRF}_{\mathcal{C}}(d)$  class. Their graphical representation in deep purple colouring is given in the folded picture by



$$\begin{array}{|c} \diagup \\ C \\ \diagdown \end{array} \begin{array}{|c} \diagdown \\ C^* \\ \diagup \end{array} \equiv \begin{array}{|c} \diagup \\ C \\ \diagdown \end{array} \Leftrightarrow \varepsilon = \sum_l C_l \otimes C_l^* \quad (4.2)$$

Figure 4.2: Definition of IRF channels in the folded picture representation

The coefficients of the Kraus operators  $\{C_l\}_{l=1,\dots,n}$  of this generalised channel are now equipped with an additional summation index  $l$  and the number of Kraus operators needed to represent

the quantum channel is bounded by  $n \leq d^3$ . Such Kraus operators take the following form

$$\mathcal{C}_l = \sum_{i,j,k,j'=1}^d (c_{ikl})_j^{j'} |i\rangle \otimes |j'\rangle \otimes |k\rangle \langle i| \otimes \langle j| \otimes \langle k| \quad (4.3)$$

In analogy to the DU-IRF subset of IRF gates which has been parameterised in §3.1.2, we now attempt to identify subsets of IRF channels which satisfy the following solvability conditions:

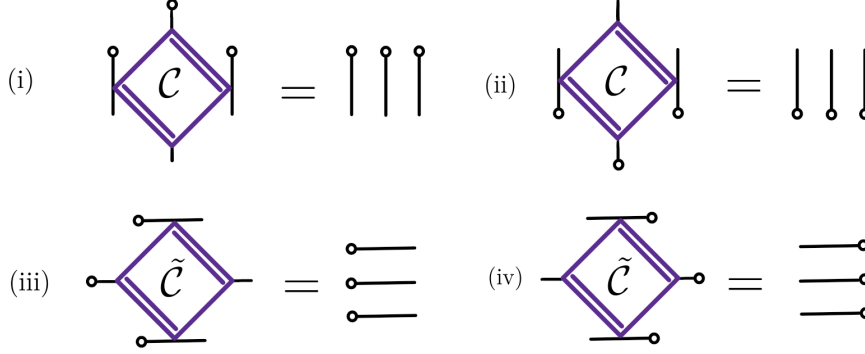


Figure 4.3: Solvability conditions of IRF channels in the folded picture

However, we will see in chapter §4.3 that in many cases not all of these conditions are necessary to ensure solvability. We hence introduce another subscript in  $\text{IRF}_{\mathcal{C},n}(d)$  indicating the number  $n$  of unitality conditions that are fulfilled by the respective subset of IRF channels. The identities from figure (4.3) translate into unitality conditions<sup>[1]</sup> along each space-time direction:

$$\begin{aligned} \text{(i)} \quad & \sum_{l=1}^n \sum_{m=1}^d (c_{ikl})_m^{j'} (c_{ikl})_j^m = \delta_{jj'} \quad \forall i, k = 1, \dots, d & \text{Trace Preservation} \\ \text{(ii)} \quad & \sum_{l=1}^n \sum_{m=1}^d (c_{ikl})_m^{j'} (c_{ikl})_j^m = \delta_{jj'} \quad \forall i, k = 1, \dots, d & \text{Time Unitality} \\ \text{(iii)} \quad & \sum_{l=1}^n \sum_{m=1}^d (\tilde{c}_{jj'l})_m^k (\tilde{c}_{jj'l})_i^m = \delta_{ik} \quad \forall j, j' = 1, \dots, d & \text{Left Unitality} \\ \text{(iv)} \quad & \sum_{l=1}^n \sum_{m=1}^d (\tilde{c}_{jj'l})_m^k (\tilde{c}_{jj'l})_i^m = \delta_{ik} \quad \forall j, j' = 1, \dots, d & \text{Right Unitality} \end{aligned}$$

with the coefficients of the dual quantum channel being related by  $(\tilde{c}_{jj'l})_i^k := (c_{ikl})_j^{j'}$ . It should be noted that condition (i) describing trace preservation, or unitality in the reversed time direction, is the only necessary condition for the quantum channel to behave physically. When imposing the other conditions (ii)-(iv), we gradually reduce the number of independent parameters in the representation of the IRF channel. One can readily see that *convex combinations* of dual unitary gates  $\sum_{l=1}^n \lambda_l u_{ikl} \otimes u_{ikl}^*$  are elements of  $\text{IRF}_{\mathcal{C},4}(d)$  because the coefficients of the corresponding channel decompose into  $c_{ikl} = \sqrt{\lambda_l} u_{ikl}$  for  $\lambda_l \geq 0$  with  $\sum_l \lambda_l = 1$  and  $u_{ik} \in \text{DU-IRF}(d)$ . For this

<sup>[1]</sup> A map  $T$  is called unital if it satisfies  $T(\mathbb{1}) = \mathbb{1}$ .

reason, non-trivial convex combinations are examples of IRF channels which preserve solvability and cannot be reduced to dual unitary dynamics. In the following we want to further restrict ourselves to the qubit case  $d = 2$  with regard to an explicit parametrisation of solvable IRF classes. In contrast to §3.1.2, a complete parametrisation of such IRF classes would even require the examination of at most 128 coefficients which does not appear to be tractable analytically. However, we note from the equations below that even the most restricted class  $\text{IRF}_{C,4}(2)$  is particularly large since it allows for up to 64 degrees of freedom in the choice of coefficients, where any gauge invariance groups have not been considered yet.

(i) *Trace Preservation* ( $d = 2$ )

$$\sum_{l=1}^n (c_{ikl}^*)_1^1 (c_{ikl})_1^1 + (c_{ikl}^*)_1^2 (c_{ikl})_1^2 = 1 \quad (4.4)$$

$$\sum_{l=1}^n (c_{ikl}^*)_1^1 (c_{ikl})_2^1 + (c_{ikl}^*)_1^2 (c_{ikl})_2^2 = 0 \quad (4.5)$$

$$\sum_{l=1}^n (c_{ikl}^*)_2^1 (c_{ikl})_1^1 + (c_{ikl}^*)_2^2 (c_{ikl})_1^2 = 0 \quad (4.6)$$

$$\sum_{l=1}^n (c_{ikl}^*)_2^1 (c_{ikl})_2^1 + (c_{ikl}^*)_2^2 (c_{ikl})_2^2 = 1 \quad (4.7)$$

(iii) *Left Unitality* ( $d = 2$ )

$$\sum_{l=1}^n (c_{1il}^*)_1^1 (c_{1kl})_1^1 + (c_{2il}^*)_1^1 (c_{2kl})_1^1 = \delta_{ik} \quad (4.8)$$

$$\sum_{l=1}^n (c_{1il}^*)_1^2 (c_{1kl})_1^2 + (c_{2il}^*)_1^2 (c_{2kl})_1^2 = \delta_{ik} \quad (4.9)$$

$$\sum_{l=1}^n (c_{1il}^*)_2^1 (c_{1kl})_2^1 + (c_{2il}^*)_2^1 (c_{2kl})_2^1 = \delta_{ik} \quad (4.10)$$

$$\sum_{l=1}^n (c_{1il}^*)_2^2 (c_{1kl})_2^2 + (c_{2il}^*)_2^2 (c_{2kl})_2^2 = \delta_{ik} \quad (4.11)$$

(ii) *Time Unitality* ( $d = 2$ )

$$\sum_{l=1}^n (c_{ikl}^*)_1^1 (c_{ikl})_1^1 + (c_{ikl}^*)_2^1 (c_{ikl})_2^1 = 1 \quad (4.12)$$

$$\sum_{l=1}^n (c_{ikl}^*)_1^1 (c_{ikl})_1^2 + (c_{ikl}^*)_2^1 (c_{ikl})_2^2 = 0 \quad (4.13)$$

$$\sum_{l=1}^n (c_{ikl}^*)_1^2 (c_{ikl})_1^1 + (c_{ikl}^*)_2^2 (c_{ikl})_2^1 = 0 \quad (4.14)$$

$$\sum_{l=1}^n (c_{ikl}^*)_1^2 (c_{ikl})_1^2 + (c_{ikl}^*)_2^2 (c_{ikl})_2^2 = 1 \quad (4.15)$$

(iv) *Right Unitality* ( $d = 2$ )

$$\sum_{l=1}^n (c_{i1l}^*)_1^1 (c_{k1l})_1^1 + (c_{i2l}^*)_1^1 (c_{k2l})_1^1 = \delta_{ik} \quad (4.16)$$

$$\sum_{l=1}^n (c_{i1l}^*)_1^2 (c_{k1l})_1^2 + (c_{i2l}^*)_1^2 (c_{k2l})_1^2 = \delta_{ik} \quad (4.17)$$

$$\sum_{l=1}^n (c_{i1l}^*)_2^1 (c_{k1l})_2^1 + (c_{i2l}^*)_2^1 (c_{k2l})_2^1 = \delta_{ik} \quad (4.18)$$

$$\sum_{l=1}^n (c_{i1l}^*)_2^2 (c_{k1l})_2^2 + (c_{i2l}^*)_2^2 (c_{k2l})_2^2 = \delta_{ik} \quad (4.19)$$

For the unitary case  $n = 1$ , one can verify that conditions (i) and (ii) imply the parametrisation (3.6) whereas conditions (iii) and (iv) correspond to the additional space unitarity constraint.

## 4.2 The Minimal Example

In the next paragraphs, we now aim to explicitly parameterise a solvable subset of IRF channels by initially reducing the number of non-zero coefficients drastically, and in the hope that efficiently many parameters remain to extract insightful examples of such channels. Following

the idea of [KS23], one may consider quantum channels  $\varepsilon$  in a subspace of the superoperator space spanned by only some of the Pauli matrices. In our case of tripartite local Hilbert space with superoperators  $\varepsilon : (\mathbb{C}^4)^{\otimes 3} \rightarrow (\mathbb{C}^4)^{\otimes 3}$ , the corresponding matrix representation of the quantum channel requires only 64 elements in the Hilbert-Schmidt normalised Pauli basis  $\{\frac{1}{2\sqrt{2}}|\sigma_\alpha \otimes \sigma_\beta \otimes \sigma_\gamma\rangle \equiv |\sigma_{\alpha\beta\gamma}\rangle\}$  with  $\alpha, \beta, \gamma \in \{0, z\}$  and  $\sigma_0 \equiv \mathbb{1}$ . Physically, such a scenario corresponds to applying local dephasing channels after the operation of each quantum channel in the IRF circuit. From there, we successively specify the matrix elements in keeping with the above-mentioned unitality conditions. One may obtain the former for a given quantum channel from the formula

$$E_{\alpha\beta\gamma}^{\alpha'\beta'\gamma'} := \text{tr}[\sigma_{\alpha'\beta'\gamma'} \varepsilon(\sigma_{\alpha\beta\gamma})] \quad \text{where} \quad \varepsilon(\cdot) = \sum_{\{\alpha\beta\gamma, \alpha'\beta'\gamma'=0,z\}} \sigma_{\alpha'\beta'\gamma'} \text{tr}(\cdot \sigma_{\alpha\beta\gamma}) E_{\alpha\beta\gamma}^{\alpha'\beta'\gamma'} \quad (4.20)$$

which renders the following matrix representation:

$$\varepsilon = \begin{pmatrix} E_{000}^{000} & E_{z00}^{000} & E_{0z0}^{000} & E_{00z}^{000} & E_{zz0}^{000} & E_{z0z}^{000} & E_{0zz}^{000} & E_{zzz}^{000} \\ E_{000}^{z00} & E_{z00}^{z00} & E_{0z0}^{z00} & E_{00z}^{z00} & E_{zz0}^{z00} & E_{z0z}^{z00} & E_{0zz}^{z00} & E_{zzz}^{z00} \\ E_{000}^{0z0} & E_{z00}^{0z0} & E_{0z0}^{0z0} & E_{00z}^{0z0} & E_{zz0}^{0z0} & E_{z0z}^{0z0} & E_{0zz}^{0z0} & E_{zzz}^{0z0} \\ E_{000}^{00z} & E_{z00}^{00z} & E_{0z0}^{00z} & E_{00z}^{00z} & E_{zz0}^{00z} & E_{z0z}^{00z} & E_{0zz}^{00z} & E_{zzz}^{00z} \\ E_{000}^{zz0} & E_{z00}^{zz0} & E_{0z0}^{zz0} & E_{00z}^{zz0} & E_{zz0}^{zz0} & E_{z0z}^{zz0} & E_{0zz}^{zz0} & E_{zzz}^{zz0} \\ E_{000}^{z0z} & E_{z00}^{z0z} & E_{0z0}^{z0z} & E_{00z}^{z0z} & E_{zz0}^{z0z} & E_{z0z}^{z0z} & E_{0zz}^{z0z} & E_{zzz}^{z0z} \\ E_{000}^{0zz} & E_{z00}^{0zz} & E_{0z0}^{0zz} & E_{00z}^{0zz} & E_{zz0}^{0zz} & E_{z0z}^{0zz} & E_{0zz}^{0zz} & E_{zzz}^{0zz} \\ E_{000}^{zzz} & E_{z00}^{zzz} & E_{0z0}^{zzz} & E_{00z}^{zzz} & E_{zz0}^{zzz} & E_{z0z}^{zzz} & E_{0zz}^{zzz} & E_{zzz}^{zzz} \end{pmatrix} \quad (4.21)$$

The explicit computation of this so-called minimal example is outsourced to the appendix A.3. As expected, we note that from trace preservation (i), the first row is immediately fixed to zero except for the first entry. Furthermore, due to the specific delta-tensor structure of the IRF channel on the left and right Hilbert spaces, the same condition allows to eliminate even more coefficients. Without any further constraints, this corresponds to the matrix (4.22) below.

$$\varepsilon = \begin{pmatrix} 1 & 0 & 0 & 0 & 0 & 0 & 0 & 0 \\ 0 & 1 & 0 & 0 & 0 & 0 & 0 & 0 \\ \mu & \mu & \zeta & \mu & \nu & \mu & \xi & a \\ 0 & 0 & 0 & 1 & 0 & 0 & 0 & 0 \\ \mu & \mu & \nu & \mu & \zeta & \mu & a & \xi \\ 0 & 0 & 0 & 0 & 0 & 1 & 0 & 0 \\ \mu & \mu & \xi & \mu & a & \mu & \zeta & \nu \\ \mu & \mu & a & \mu & \xi & \mu & \nu & \zeta \end{pmatrix} \quad (4.22)$$

If one allows for time unitality (ii), not only the first column vanishes, but also several other sites with coefficients  $\mu$ . In addition, the left unitality condition (iii) eliminates coefficients  $\xi$  whereas the right unitality condition (iv) sets all  $\nu$  to zero. Eventually, we introduce the letter  $\zeta$  for coefficients that yield zero for either or both of the conditions (iii) and (iv). Assuming all unitality conditions, this subset of quantum channels possesses exactly one free parameter  $a$ . In the scenario of only three fulfilled unitality conditions, this solvable subset extends to a 2-parametric set  $\{a, \nu\}$  for left unital, or  $\{a, \xi\}$  for right unital quantum channels respectively. In any case, one still needs to verify complete positivity of the quantum channel for the specific choice of parameter values, which will be addressed later in this chapter.

Let us firstly analyse and interpret our intermediate result by graphically confirming our computations. That is, we would like to understand why only such coefficients remain in the 4-way unital case where the indices satisfy  $\alpha \neq \alpha', \beta = \beta' = z$  and  $\gamma \neq \gamma'$ . For this purpose we draw the TNN representation of equation (4.20) in the unfolded picture to make explicit use of delta-tensor manipulations. The restriction to the diagonal matrices  $\sigma_0 = \mathbb{1}$  and  $\sigma_z$  gives rise to four scenarios I-IV as presented in the figure below.

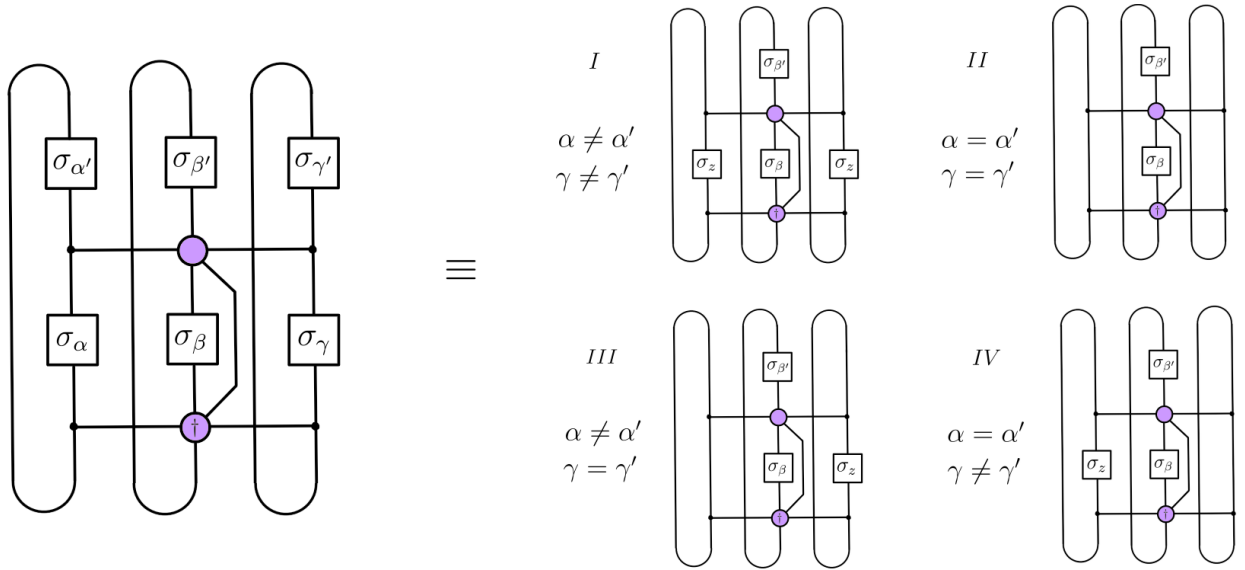


Figure 4.4: Graphical computation of the coefficients in the minimal example

It should be noticed that the appearing  $\sigma_z$  matrices may be shifted freely upwards and downwards along the outer Hilbert spaces in the pictures above. In scenario I, this property allows us to apply conditions (i) or (ii), and since  $\sigma_z$  is trace free, the network vanishes immediately. The only case where this is not possible corresponds to the choice of indices  $\beta = \beta' = z$ , as we would expect from the matrix representation (4.22). In scenario II, one finds with the same arguments that the network equals zero but for the case where both  $\beta = \beta' = 0$ , which renders

the one entries on the diagonal of the matrix. The zero contribution of the case  $\beta = \beta' = z$  clarifies after the analysis of the two other scenarios. In the scenarios III and IV, all coefficients disappear analogously except for the more complex case  $\beta = \beta' = z$ . We now remind ourselves of the form of the two space unitality constraints (iii) and (iv) in the unfolded picture. On the left hand side of the tensor network (4.5), we apply left unitality at the second equivalent sign which subsequently cancels out the coefficients with  $\beta = \beta' = z$  in scenario III. Equivalently, on the right hand side, the same procedure is executed taking advantage of the right unitality condition to make the network disappear. In case that only one of the two constraints (iii) and (iv) is applied, we gain the predicted additional degree of freedom.

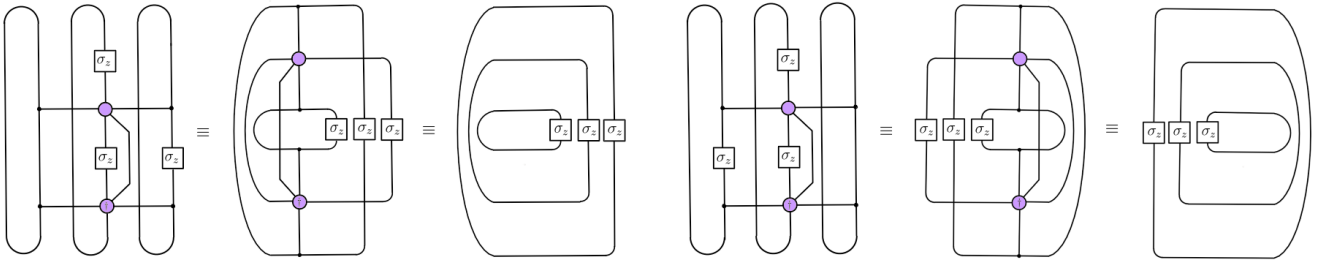


Figure 4.5: Scenario III (left) and IV (right): Application of the left (right) unitality condition

In summary, both the analytical and graphical approach yield identical results for the matrix coefficients. Let us then shortly present some immediate implications of our findings so far. From the matrix (4.22) one can conclude that some important representatives of quantum channels are not embedded in the  $\text{IRF}_C(2)$  class. Most importantly, the *Completely Depolarising Channel*  $\varepsilon(\cdot) = \text{tr}(\cdot) \frac{\mathbb{1}}{d^3}$ , as graphically defined in (4.6), is incompatible with the structure of this class. This is due to the fact that this channel would require only the element  $E_{000}^{000} = 1$  and does not allow for any further matrix coefficients with values other than zero. Moreover, one finds that also the *Dephasing Channel*  $\varepsilon(\cdot) = \Pi_{\mathcal{D}}(\cdot)$  is generally irreconcilable with additional space unitality constraints. The projector  $\Pi_{\mathcal{D}}$  on the diagonal subspace of the quantum state corresponds to an identity matrix representation which is no longer possible as soon as  $\zeta = 0$ .

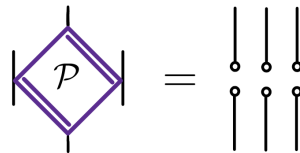


Figure 4.6: Completely Depolarising Channel in the folded picture

Let us now systematically study the action of the matrix (4.22): We recognise that we have to deal with permutation matrices intrinsically. In the case of 3-way unital channels, one may set



the parameter  $a = 0$ . Furthermore, the choice  $\nu = 1$  for left unital channels and  $\xi = 1$  for right unital channels reveals some important characteristics. In the same spirit, one may set  $a = 1$  for the case of 4-way unital quantum channels. The following TNN illustrations summarise the action of the IRF channel on the reduced Pauli basis in these three cases. In any of them, the basis states remain unchanged if  $|\sigma_0\rangle$  is acting on the middle entry of the gate.

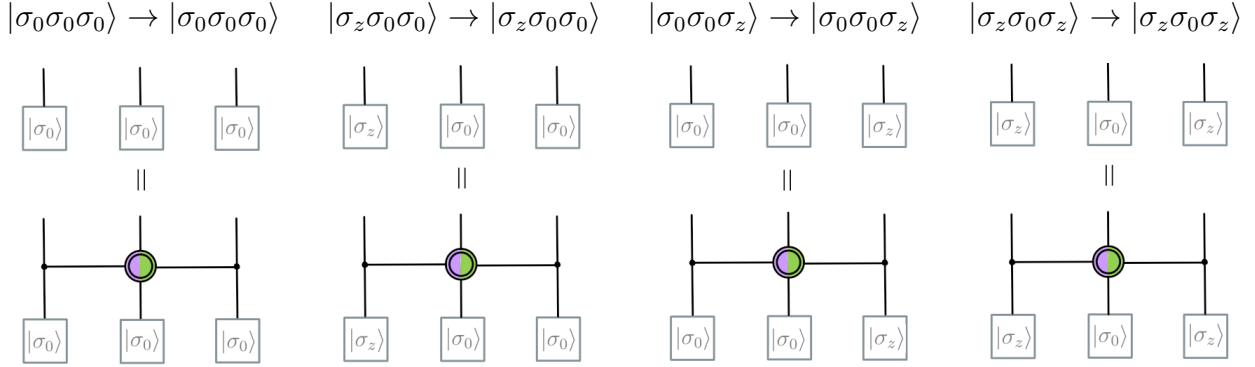


Figure 4.7: Unflipped states for 3- and 4-way unital quantum channels

Deep purple colouring again refers to the  $\text{IRF}_{C,4}(2)$  class whereas green colours highlight elements of  $\text{IRF}_{C,3}(2)$  that only satisfy one space unitality condition. The double circles on the middle tensors accent the folded picture notation.

For left unital channels, with  $a = \xi = 0$  and  $\nu = 1$ , the state on the left Hilbert space is flipped if  $|\sigma_z\rangle$  acts on the middle Hilbert space.

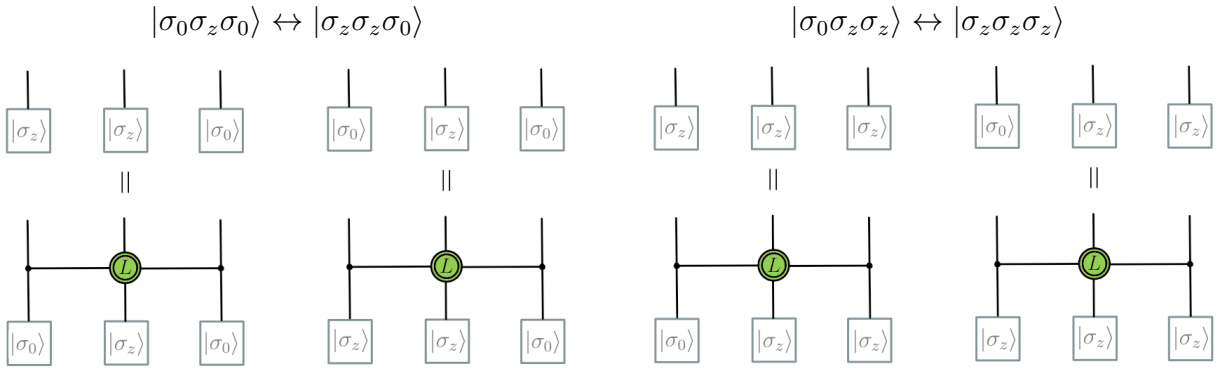


Figure 4.8:  $a = \xi = 0$  and  $\nu = 1$ : Flipped states of 3-way unital quantum channels

Conversely, for the right unital case with  $a = \nu = 0$  and  $\xi = 1$ , the flipping is only performed on the right Hilbert space if  $|\sigma_z\rangle$  enters in the middle position:

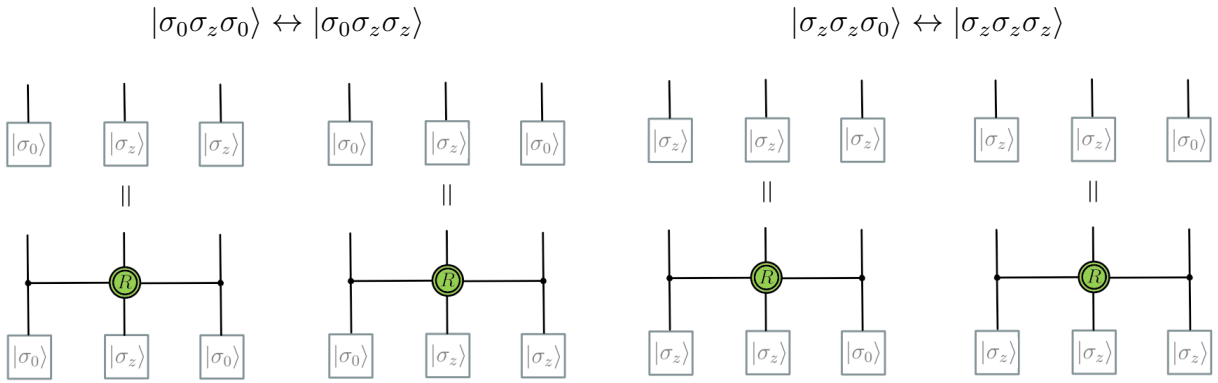


Figure 4.9:  $a = \nu = 0$  and  $\xi = 1$ : Flipped states of 3-way unital quantum channels

For 4-way unital quantum channels, where  $\xi = \nu = 0$ , the choice  $a = 1$  yields both flipping operations on the outer Hilbert spaces when  $|\sigma_z\rangle$  is applied on the middle entry.

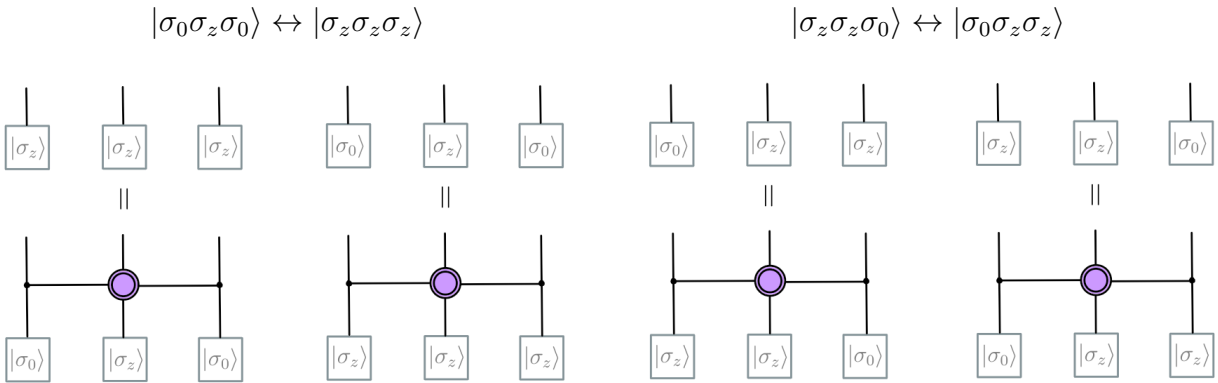


Figure 4.10:  $a = 1$  and  $\xi = \nu = 0$ : Flipped states of 4-way unital quantum channels

In conclusion, we have shown that these parametrisations allow an interpretation in terms of *Controlled NOT* (CNOT) gates if we map  $|\sigma_0\rangle \mapsto |0\rangle$  and  $|\sigma_z\rangle \mapsto |1\rangle$ .

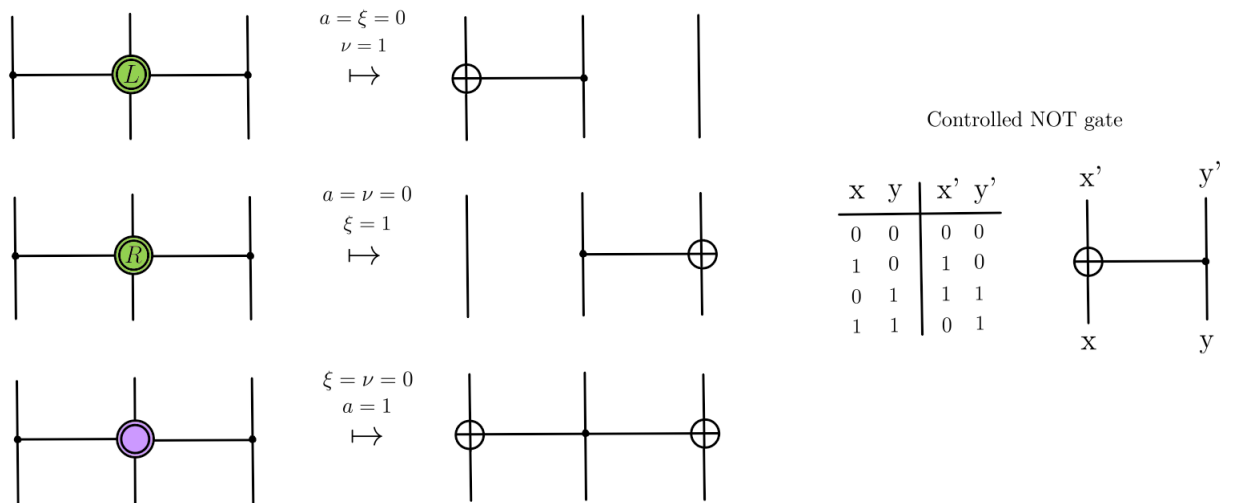


Figure 4.11: Identification with Controlled NOT gates of 3- and 4-way unital IRF-channels

With this knowledge, we are now also in a position to further specify the structure of the folded middle tensors of figure (4.11). As summarised in figure (4.12), one can assign to the middle tensor another reduced tensor  $L'$ , or  $R'$  respectively, whose two non-zero components completely determine the action of the 3-way unital IRF-channel. These middle tensors are the fundamental objects of this class of quantum channels because both the IRF-gate and its dual can be constructed by simply adding the delta tensors at their respective positions. It should be mentioned that our examples of  $\text{IRF}_{\mathcal{C},3}(2)$  may not be produced by convex combinations of DUIRF gates since these would imply 4-way unitality immediately. This might not be the case for our example of  $\text{IRF}_{\mathcal{C},4}(2)$ .

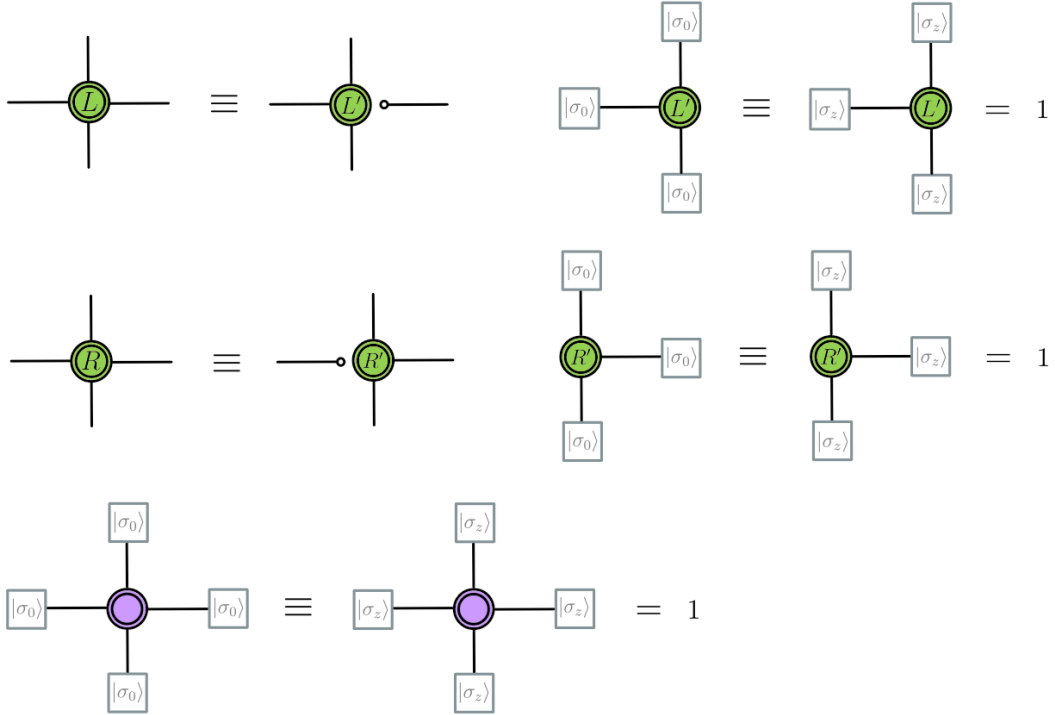


Figure 4.12: Characterisation of the middle tensor of 3- and 4-way unital IRF-channels

Let us now briefly sketch the computation of the respective Choi state  $\sigma^\varepsilon$  which is required for the verification of complete positivity of our examples of IRF quantum channels. We make use of the fact that a quantum channel is completely positive if the corresponding  $\sigma^\varepsilon$  has a positive semi-definite matrix representation. Let us firstly recall the definition of the Choi state:  $\sigma^\varepsilon = (\varepsilon \otimes \mathbb{1}_8)(|\Psi\rangle\langle\Psi|) = \sum_{i,j=1}^8 \varepsilon(|i\rangle\langle j|) \otimes |i\rangle\langle j|$ , expressed in the 8-dimensional computational basis. Inserting definition (4.20) and using the fact that we have restricted us to the reduced Pauli basis where  $\langle i|\sigma_{\alpha\beta\gamma}|j\rangle = 0$  for  $i \neq j$ , we only need to evaluate the diagonal terms. For the three examples the resulting expression  $\sigma^\varepsilon = \sum_{\{\alpha\beta\gamma,\alpha'\beta'\gamma'=0,z\}} \sum_i \langle i|\sigma_{\alpha\beta\gamma}|i\rangle E_{\alpha\beta\gamma}^{\alpha'\beta'\gamma'} (\sigma_{\alpha'\beta'\gamma'} \otimes |i\rangle\langle i|)$  yields contributions for exactly 8 non-zero matrix coefficients  $E_{\alpha\beta\gamma}^{\alpha'\beta'\gamma'}$ . It was checked with Mathematica that  $\sigma^\varepsilon$  is indeed positive semi-definite for the above-mentioned combinations of parameter values, that is, we have found new valid quantum channels.

### 4.3 Solvability of IRF Channel Circuits

In contrast to quantum circuits of unitary gates which may have an additional space unitarity property, we can distinguish several more classes in the realm of networks of quantum channels. All of them have to obey the trace preservation condition (i) but may beyond that include any of the other unitality conditions (ii), (iii) and (iv). In the same way as for conventional bipartite quantum gates discussed in [KS23], we mostly focus on the analysis of *3-way unital* quantum channels since they still guarantee solvability in many applications. This class imposes condition (ii) and either of the conditions (iii) and (iv) such that it possesses more degrees of freedom than generic 4-way unital channels, and therefore is more general. For illustration purposes, one may again consider the computation of spatio-temporal correlation functions from chapter §3.2.1. This time, we replace the unitary gates with IRF quantum channels:

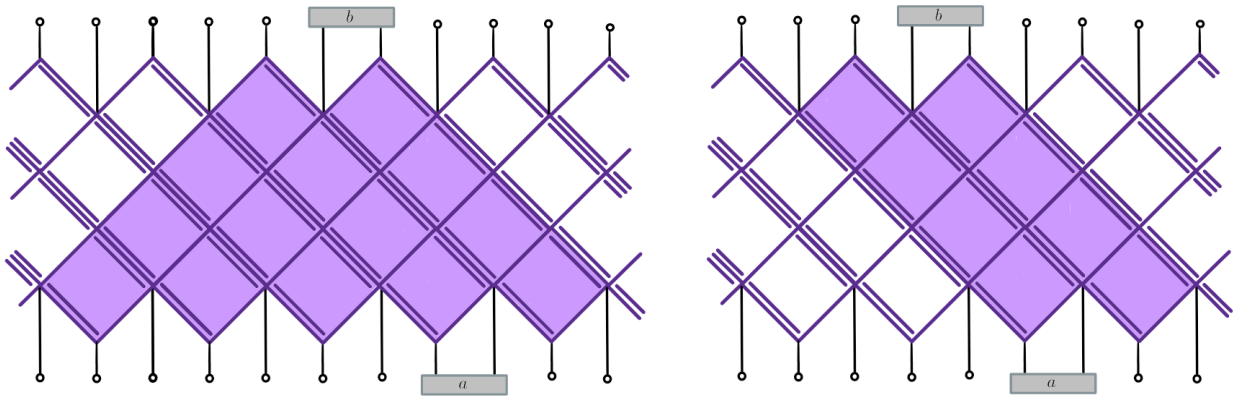


Figure 4.13: Computation of spatio-temporal correlation functions of IRF channel circuits

On the left hand side of figure (4.13) we have only applied the trace preservation condition (i) which reduces the quantum circuit to the deep purple coloured faces. Next to it we further imposed time unitality (ii) which produces an identical picture to circuits of unitary IRF gates (3.9). Other than in the latter, we now have two different possibilities to contract the circuit space-wise by either applying the left unitality (iii) or right unitality (iv) condition:

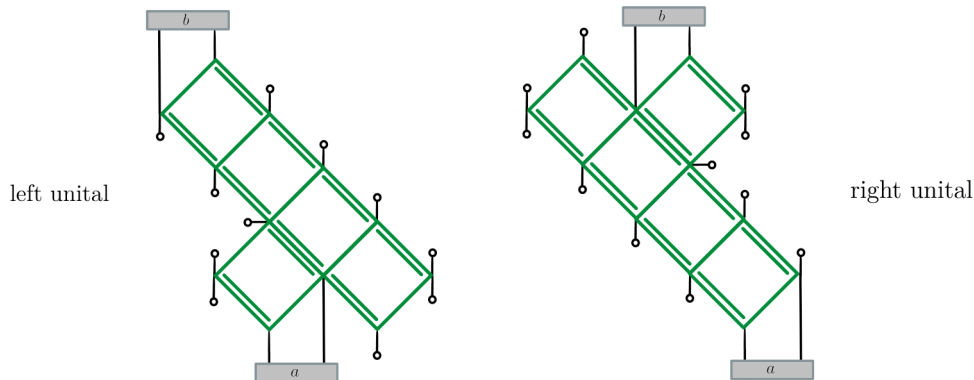


Figure 4.14: Reduced circuits for left or right unital IRF channels

In analogy to (3.10), one may again find correlation maps that give explicit solutions to the remaining network of tensors. Most importantly, one realises that there are more non-vanishing correlations than in the dual-unitary or 4-way unital setup. Namely, figure (4.14) suggests that such correlations may exist for any position of the lower observable  $a$  such that the light cone of the upper observable  $b$  completely encloses the support of  $a$ . The linear shape of the remaining tensor network renders this problem exactly solvable for only 3-way unital quantum channels.



---

## Conclusion and Outlook

---

In this work, we have reviewed the notion of quantum channels and how implementations of these into quantum circuits allow for the analysis of noisy dynamics. In contrast to the DUIRF model, a complete parametrisation of the class of IRF quantum channels  $\text{IRF}_{\mathcal{C}}(d)$  over qudits does not seem to be tractable analytically. However, by restricting ourselves to a solvable subset of the qubit case ( $d = 2$ ), we have gained valuable insights into the structure of this class. It could be shown that the Completely Depolarising Channel does not respect the structure of IRF quantum channels and that the Dephasing Channel is incompatible with any additional space unitality conditions. Furthermore, we elaborated on the specific structure of examples in  $\text{IRF}_{\mathcal{C},3}(2)$  that go even beyond convex combinations of DUIRF gates which always proved to be included in  $\text{IRF}_{\mathcal{C}}(d)$  for any local Hilbert space dimension  $d$ . Interestingly, our examples of IRF channels are in one-to-one correspondence to specific constructions of CNOT gates.

It remains for future work to explore the scope of application and the advantages of circuits constructed by these gates. Moreover, it might be of interest to find the Kraus operators for our examples which follow from the diagonalisation of the corresponding Choi matrices. This would clarify whether our example in  $\text{IRF}_{\mathcal{C},4}(2)$  can be written in terms of convex combinations of DUIRF gates or possesses other interesting features. It could also be illuminating to study the existence of IRF channels for a different combination of parameter values for  $\{a, \xi, \nu\}$ .

Another step in the characterisation of this class could be to develop perturbatively around elements of  $\text{IRF}_{\mathcal{C}}(d)$  to such an extent that complete positivity and solvability are still preserved. This could reveal generic structural information about IRF channels and turned out to be a rewarding approach in the case of circuits of bipartite quantum channels in [KS23]. Similarly to [CLV23], where a formalism has been developed to collectively describe both dual-unitary gates with bi- and tripartite support, one may ask if such description would also extend to quantum channels.





# APPENDIX A

---

## Explanatory Notes and Computations

---

### A.1 The Relative State Method

The idea of the *Relative State Method* is to completely determine the action of an operator  $\mathcal{A}$  over  $\mathcal{H} \equiv \mathcal{H}_{int}$  by looking at the larger Hilbert space  $\mathcal{H} \otimes \mathcal{H}_{ext}$ . It can be shown that it suffices to describe the action of  $\mathcal{A} \otimes \mathbb{1}_{ext}$  on a single pure maximally entangled state in the composite Hilbert space. We therefore consider<sup>[1]</sup>

$$|\Psi\rangle = \frac{1}{\sqrt{n}} \sum_{i=1}^n |\alpha_i\rangle_{int} \otimes |\beta_i\rangle_{ext} \quad (\text{A.1})$$

where we assume that  $\dim(\mathcal{H}_{ext}) \equiv d \geq \dim(\mathcal{H}) \equiv n$ . The states  $\{|\alpha_i\rangle_{int}\}_{i=1}^n$  and  $\{|\beta_i\rangle_{ext}\}_{i=1}^d$  are chosen to form an orthonormal basis on  $\mathcal{H}$  and  $\mathcal{H}_{ext}$  respectively. One can express any state in  $\mathcal{H}$  as  $|\phi\rangle_{int} = \sum_{i=1}^n c_i |\alpha_i\rangle_{int}$  with  $\sum_{i=1}^n |c_i|^2 = 1$ . Equally, we obtain the same state by partially contracting the composite system

$$\frac{1}{\sqrt{n}} |\phi\rangle_{int} = {}_{ext} \langle \phi^* | \Psi \rangle \quad \text{with} \quad |\phi^*\rangle_{ext} = \sum_{i=1}^n c_i^* |\beta_i\rangle_{ext} \quad (\text{A.2})$$

where we have identified the relative state  $|\phi\rangle_{int}$  with respect to an index state  $|\phi^*\rangle_{ext}$ . They are related by an antilinear and antiunitary map  $|\phi\rangle_{int} \mapsto |\phi^*\rangle_{ext}$  between  $\mathcal{H}$  and a  $n$ -dimensional subspace of  $\mathcal{H}_{ext}$ . If we act with local operators  $\mathcal{A} \otimes \mathbb{1}_{ext}$  on our composite state and again contract the external Hilbert space, we are left with the relative state

$${}_{ext} \langle \phi^* | (\mathcal{A} \otimes \mathbb{1}_{ext}) | \Psi \rangle = \frac{1}{\sqrt{n}} \mathcal{A} |\phi\rangle_{int} \quad (\text{A.3})$$

In conclusion, we have realized the local operation  $\mathcal{A}$  on an extended maximally entangled

---

<sup>[1]</sup>  $|\Psi\rangle$  is maximally entangled since  $\text{tr}_{\mathcal{H}_{ext}}(|\Psi\rangle \langle \Psi|) \propto \mathbb{1}_n$

state and found that the state  $|\phi\rangle_{int}$  is prepared if the outcome of the measurement in  $\mathcal{H}_{ext}$  is  $|\phi^*\rangle_{ext}$ . We will use this result to show that every quantum channel has a Kraus decomposition by applying the relative state method to superoperators in chapter §2.1.2.

## A.2 Purification of Quantum States

In order to prove that any Kraus representation relates to a unique quantum channel, we need to introduce the purification of a quantum state. The GHJW theorem which characterises such purifications in [Pre98] can be understood elegantly in TNN as described in [BC17]. If we have a generic quantum state  $\rho \in \mathcal{H}$  decomposed into an ensemble of pure states  $|\Phi_k\rangle \in \mathcal{H}$

$$\rho = \sum_k q_k |\Phi_k\rangle \langle \Phi_k| \quad (\text{A.4})$$

with coefficients  $q_k \geq 0$  such that  $\sum_k q_k = 1$ , then such quantum state can be thought of as the partial trace of a pure state in a larger Hilbert space  $\mathcal{H} \otimes \mathcal{H}_{pur}$ . The extension  $\mathcal{H}_{pur}$  is called the purification space. For some mutually orthogonal and normalized  $|\gamma_k\rangle_{pur}$  we may write

$$\rho = \text{tr}_{\mathcal{H}_{pur}}(|\Upsilon\rangle)(\langle \Upsilon|) \quad \text{where} \quad |\Upsilon\rangle = \sum_k \sqrt{q_k} |\Phi_k\rangle \otimes |\gamma_k\rangle_{pur} \quad (\text{A.5})$$

having identified  $|\Upsilon\rangle$  as the *purification* of  $\rho$ . In graphical notation, when grouping the  $k$  indices in both spaces, purification implies the equation

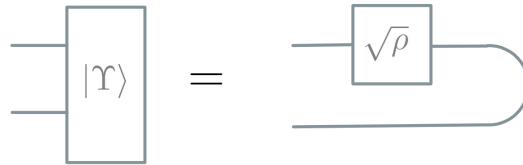


Figure A.1: Purification of a density operator in TNN

and partially tracing over the purification space yields the original quantum state as desired:

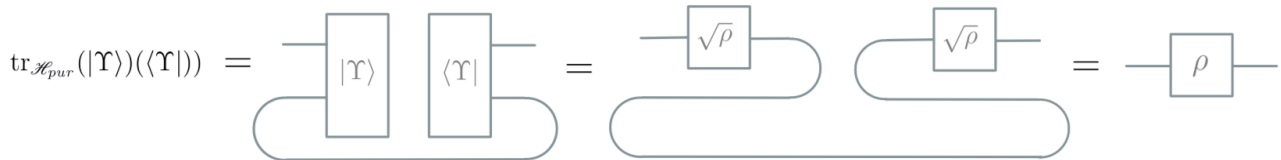


Figure A.2: Partial trace of a purified quantum state in TNN

When performing the partial trace, one readily notices that purification is unique up to a unitary freedom on the purification space  $|\gamma_k\rangle_{pur} \mapsto U_{pur} |\gamma_k\rangle_{pur}$  where  $U_{pur}^\dagger U_{pur} = \mathbb{1}$ . The so-

called *GHJW theorem*<sup>[2]</sup> summarises this observation: If we have two realisations of the same quantum state in terms of mixed states  $\rho = \sum_k q_k |\Phi_k\rangle\langle\Phi_k|$  and  $\rho = \sum_{k'} p_{k'} |\Phi'_{k'}\rangle\langle\Phi'_{k'}|$ , then their corresponding purifications read

$$|\Upsilon\rangle = \sum_k \sqrt{q_k} |\Phi_k\rangle \otimes |\gamma_k\rangle_{pur} \quad \text{and} \quad |\Upsilon'\rangle = \sum_{k'} \sqrt{p_{k'}} |\Phi'_{k'}\rangle \otimes |\delta_{k'}\rangle_{pur} \quad (\text{A.6})$$

given two different orthonormal bases  $\{|\gamma_k\rangle_{pur}\}_{k=1}^m$  and  $\{|\delta_{k'}\rangle_{pur}\}_{k'=1}^m$  for  $\dim(\mathcal{H}_{pur}) = m$ . The GHJW theorem states that purifications of the same quantum state are necessarily linked by a unitary transformation in order for the density operators to be indistinguishable.

$$|\Upsilon'\rangle = (\mathbb{1} \otimes U_{pur}) |\Upsilon\rangle \quad (\text{A.7})$$

Practically this means that one can prepare the different ensembles of a mixed state by only acting on the purifying system such that the density operators remains unchanged.

### A.3 Computations of the Minimal Example

Here we provide explicit computations for the minimal example of chapter §4.1. The coefficients of the quantum channel are given by equation (4.20) that is repeated hereafter

$$E_{\alpha\beta\gamma}^{\alpha'\beta'\gamma'} := \text{tr} [\sigma_{\alpha'\beta'\gamma'} \varepsilon(\sigma_{\alpha\beta\gamma})] \quad (\text{A.8})$$

We simplify the upper equation by only allowing for matrices  $\sigma_0$  and  $\sigma_z$  on the local Hilbert spaces. Inserting the formula (4.2) and (4.3) for the superoperator yields the following expression<sup>[3]</sup>, up to an omitted prefactor of  $(\frac{1}{2\sqrt{2}})^2$  for the normalisation.

$$\begin{aligned} E_{\alpha\beta\gamma}^{\alpha'\beta'\gamma'} &= \langle\sigma_{\alpha'\beta'\gamma'}| \sum_l \mathcal{C}_l \otimes \mathcal{C}_l^* |\sigma_{\alpha\beta\gamma}\rangle \\ &= \left[ \langle\Omega| (\sigma_{\alpha'} \otimes \mathbb{1}) \otimes \langle\Omega| (\sigma_{\beta'} \otimes \mathbb{1}) \otimes \langle\Omega| (\sigma_{\gamma'} \otimes \mathbb{1}) \right] \left[ \sum_l \sum_{ijkj'} \sum_{mnrn'} (c_{ikl})_j^{j'} (c_{mrl})_n^{n'} (|i\rangle\langle i| \otimes |m\rangle\langle m|) \right. \\ &\quad \left. \otimes (|j'\rangle\langle j| \otimes |n'\rangle\langle n|) \otimes (|k\rangle\langle k| \otimes |r\rangle\langle r|) \right] \left[ (\sigma_\alpha \otimes \mathbb{1}) |\Omega\rangle \otimes (\sigma_\beta \otimes \mathbb{1}) |\Omega\rangle \otimes (\sigma_\gamma \otimes \mathbb{1}) |\Omega\rangle \right] \\ &= \sum_l \sum_{ijkj'} \sum_{mnrn'} (c_{ikl})_j^{j'} (c_{mrl})_n^{n'} \langle\Omega| (\sigma_{\alpha'} |i\rangle\langle i| \sigma_\alpha \otimes |m\rangle\langle m|) |\Omega\rangle \cdot \langle\Omega| (\sigma_{\beta'} |j'\rangle\langle j| \sigma_\beta \otimes |n'\rangle\langle n|) |\Omega\rangle \\ &\quad \cdot \langle\Omega| (\sigma_{\gamma'} |k\rangle\langle k| \sigma_\gamma \otimes |r\rangle\langle r|) |\Omega\rangle \end{aligned}$$

In a first step, we evaluate the value of the matrix coefficient  $E_{000}^{000}$ :

<sup>[2]</sup> The GHJW theorem is named after the physicists and mathematicians Nicolas Gisin, Lane P. Hughston, Richard Jozsa and William Wootters.

<sup>[3]</sup> Here we used the formula  $|A\rangle = (A \otimes \mathbb{1}) |\Omega\rangle$  where  $|\Omega\rangle \equiv |\Phi^+\rangle$  corresponds to the first Bell state.

$$\begin{aligned}
E_{000}^{000} &= \sum_l \sum_{ijkj'} \sum_{mnrn'} (c_{ikl})_j^{j'} (c_{mrl})_n^{n'} \langle \Omega | (|i\rangle \langle i| \otimes |m\rangle \langle m|) | \Omega \rangle \cdot \langle \Omega | (|j'\rangle \langle j| \otimes |n'\rangle \langle n|) | \Omega \rangle \\
&\quad \cdot \langle \Omega | (|k\rangle \langle k| \otimes |r\rangle \langle r|) | \Omega \rangle \\
&= \sum_l \sum_{ijkj'} \sum_{mnrn'} (c_{ikl})_j^{j'} (c_{mrl})_n^{n'} \delta_{im} \delta_{jn} \delta_{j'n'} \delta_{kr} \\
&= \sum_{ik} \sum_l \sum_{jj'} (c_{ikl})_j^{j'} (c_{ikl})_j^{j'}
\end{aligned}$$

By applying the trace preservation condition (i) we obtain the value  $E_{000}^{000} = 1$ . Furthermore, one finds that the latter condition also implies that  $E_{\alpha\beta\gamma}^{000} = 0$  except for the case where all indices are zero. More generally, we note that the following identities hold

$$\begin{aligned}
\langle \Omega | (\sigma_{\alpha'} |i\rangle \langle i| \sigma_{\alpha} \otimes |m\rangle \langle m|) | \Omega \rangle &= \delta_{\alpha=\alpha'} \delta_{im} + \delta_{\alpha \neq \alpha'} (\delta_{i1} \delta_{m1} - \delta_{i2} \delta_{m2}) \\
\langle \Omega | (\sigma_{\beta'} |j\rangle \langle j'| \sigma_{\beta} \otimes |n\rangle \langle n'|) | \Omega \rangle &= \delta_{jn} \delta_{j'n'} [\delta_{\beta 1} \delta_{\beta' 1} + \delta_{\beta 2} \delta_{\beta' 2} (\delta_{j1} \delta_{j'1} + \delta_{j2} \delta_{j'2} - \delta_{j2} \delta_{j'1} - \delta_{j1} \delta_{j'2}) \\
&\quad + \delta_{\beta 2} \delta_{\beta' 1} (\delta_{j1} \delta_{j'1} - \delta_{j2} \delta_{j'2} - \delta_{j2} \delta_{j'1} + \delta_{j1} \delta_{j'2}) \\
&\quad + \delta_{\beta 1} \delta_{\beta' 2} (\delta_{j1} \delta_{j'1} - \delta_{j2} \delta_{j'2} + \delta_{j2} \delta_{j'1} - \delta_{j1} \delta_{j'2})] \\
\langle \Omega | (\sigma_{\gamma'} |i\rangle \langle i| \sigma_{\gamma} \otimes |m\rangle \langle m|) | \Omega \rangle &= \delta_{\gamma=\gamma'} \delta_{kr} + \delta_{\gamma \neq \gamma'} (\delta_{k1} \delta_{r1} - \delta_{k2} \delta_{r2})
\end{aligned}$$

The structure of this particular quantum channel immediately also cancels out coefficients  $E_{\alpha z \gamma}^{\alpha' 0 \gamma'}$  for any choice of the other indices. Let us for instance examine the coefficient  $E_{0z0}^{000}$ :

$$\begin{aligned}
E_{0z0}^{000} &= \sum_l \sum_{ijkj'} \sum_{mnrn'} (c_{ikl})_j^{j'} (c_{mrl})_n^{n'} \langle \Omega | (|i\rangle \langle i| \otimes |m\rangle \langle m|) | \Omega \rangle \cdot \langle \Omega | (|j'\rangle \langle j| \sigma_z \otimes |n'\rangle \langle n|) | \Omega \rangle \\
&\quad \cdot \langle \Omega | (|k\rangle \langle k| \otimes |r\rangle \langle r|) | \Omega \rangle \\
&= \sum_l \sum_{ijkj'} \sum_{mnrn'} \delta_{im} \delta_{jn} \delta_{j'n'} (\delta_{j1} \delta_{j'1} - \delta_{j2} \delta_{j'2} - \delta_{j2} \delta_{j'1} + \delta_{j1} \delta_{j'2}) \delta_{kr} \\
&= \sum_l \sum_{ik} [(c_{ikl})_1^1 (c_{ikl})_1^1 - (c_{ikl})_2^2 (c_{ikl})_2^2 - (c_{ikl})_2^1 (c_{ikl})_1^2 + (c_{ikl})_1^2 (c_{ikl})_1^1]
\end{aligned}$$

which vanishes with trace preservation. In the same manner, such calculations can be retraced for all the other combinations of indices, still only taking advantage of the first condition.

If we additionally assume time unitality (ii), all the coefficients  $E_{000}^{\alpha' \beta' \gamma'}$  but for the very first matrix entry cancel out. Let us further illustrate that coefficients  $E_{\alpha 0 \gamma}^{\alpha' z \gamma'}$  are set to zero by this condition as well. For example one may compute  $E_{z00}^{0z0}$ :

$$\begin{aligned}
E_{z00}^{0z0} &= \sum_l \sum_{ijkj'} \sum_{mnrn'} (c_{ikl})_j^{j'} (c_{mrl})_n^{n'} \langle \Omega | (|i\rangle \langle i| \sigma_z \otimes |m\rangle \langle m|) | \Omega \rangle \cdot \langle \Omega | (\sigma_z |j'\rangle \langle j| \otimes |n'\rangle \langle n|) | \Omega \rangle \\
&\quad \cdot \langle \Omega | (|k\rangle \langle k| \otimes |r\rangle \langle r|) | \Omega \rangle \\
&= \sum_l \sum_{ijkj'} \sum_{mnrn'} (c_{ikl})_j^{j'} (c_{mrl})_n^{n'} (\delta_{i1} \delta_{m1} - \delta_{i2} \delta_{m2}) \delta_{jn} \delta_{j'n'} (\delta_{j1} \delta_{j'1} - \delta_{j2} \delta_{j'2} + \delta_{j2} \delta_{j'1} - \delta_{j1} \delta_{j'2}) \delta_{kr}
\end{aligned}$$

$$\begin{aligned}
&= \sum_k \sum_l [(c_{1kl})_1^1 (c_{1kl}^*)_1^1 - (c_{2kl})_1^1 (c_{2kl}^*)_1^1 - (c_{1kl})_2^2 (c_{1kl}^*)_2^2 + (c_{2kl})_2^2 (c_{2kl}^*)_2^2 + (c_{1kl})_2^1 (c_{1kl}^*)_2^1 \\
&\quad - (c_{2kl})_2^1 (c_{2kl}^*)_2^1 - (c_{1kl})_1^2 (c_{1kl}^*)_1^2 + (c_{2kl})_1^2 (c_{2kl}^*)_1^2]
\end{aligned}$$

which equals zero under the assumption of time unitality. One can further check that either or both of the conditions (i) and (ii) implies that  $E_{\alpha 0 \gamma}^{\alpha' 0 \gamma'} = 0$  except for the case  $E_{\alpha 0 \gamma}^{\alpha 0 \gamma} = 1$ .

Eventually, the quantum channel may also be taken left unital (iii) such that coefficients  $E_{\alpha z \gamma}^{\alpha z \gamma'}$  disappear. For the right unital case (iv) we obtain  $E_{\alpha z \gamma}^{\alpha' z \gamma} = 0$  respectively. This is demonstrated exemplarily for the case of  $E_{0z0}^{zz0}$ :

$$\begin{aligned}
E_{0z0}^{zz0} &= \sum_l \sum_{ijkj'} \sum_{mnrn'} (c_{ikl})_j^{j'} (c_{mrl})_n^{n'} \langle \Omega | (\sigma_z |i\rangle \langle i| \otimes |m\rangle \langle m|) | \Omega \rangle \cdot \langle \Omega | (\sigma_z |j'\rangle \langle j| \sigma_z \otimes |n'\rangle \langle n|) | \Omega \rangle \\
&\quad \cdot \langle \Omega | (|k\rangle \langle k| \sigma_z \otimes |r\rangle \langle r|) | \Omega \rangle \\
&= \sum_l \sum_{ijkj'} \sum_{mnrn'} (c_{ikl})_j^{j'} (c_{mrl})_n^{n'} (\delta_{i1} \delta_{m1} - \delta_{i2} \delta_{m2}) \delta_{jn} \delta_{j'n'} (\delta_{j1} \delta_{j'1} + \delta_{j2} \delta_{j'2} - \delta_{j2} \delta_{j'1} - \delta_{j1} \delta_{j'2}) \delta_{kr} \\
&= \sum_l \sum_k [(c_{1kl})_1^1 (c_{1kl}^*)_1^1 - (c_{2kl})_1^1 (c_{2kl}^*)_1^1 + (c_{1kl})_2^2 (c_{1kl}^*)_2^2 - (c_{2kl})_2^2 (c_{2kl}^*)_2^2 - (c_{1kl})_2^1 (c_{1kl}^*)_2^1 \\
&\quad + (c_{2kl})_2^1 (c_{2kl}^*)_2^1 - (c_{1kl})_1^2 (c_{1kl}^*)_1^2 + (c_{2kl})_1^2 (c_{2kl}^*)_1^2]
\end{aligned}$$

If one carries out the two sums, each term equals one which in total yields the result zero. We give a summary of all the 64 coefficients in the matrix representation (4.22). In chapter §4.1, we also provide another graphical approach to these computations for verification purposes.



---

## Bibliography

---

- [KS23] Pavel Kos and Georgios Styliaris. “Circuits of space and time quantum channels”. In: *Quantum* 7 (May 2023), p. 1020. ISSN: 2521-327X. DOI: [10.22331/q-2023-05-24-1020](https://doi.org/10.22331/q-2023-05-24-1020). URL: <http://dx.doi.org/10.22331/q-2023-05-24-1020>.
- [Pro21] Tomaž Prosen. “Many-body quantum chaos and dual-unitarity round-a-face”. In: *Chaos: An Interdisciplinary Journal of Nonlinear Science* 31.9 (Sept. 2021). ISSN: 1089-7682. DOI: [10.1063/5.0056970](https://doi.org/10.1063/5.0056970). URL: <http://dx.doi.org/10.1063/5.0056970>.
- [CLV23] Pieter W. Claeys, Austen Lamacraft, and Jamie Vicary. *From dual-unitary to biunitary: a 2-categorical model for exactly-solvable many-body quantum dynamics*. 2023. arXiv: [2302.07280](https://arxiv.org/abs/2302.07280) [[quant-ph](#)].
- [BC17] Jacob C Bridgeman and Christopher T Chubb. “Hand-waving and interpretive dance: an introductory course on tensor networks”. In: *Journal of Physics A: Mathematical and Theoretical* 50.22 (May 2017), p. 223001. ISSN: 1751-8121. DOI: [10.1088/1751-8121/aa6dc3](https://doi.org/10.1088/1751-8121/aa6dc3). URL: <http://dx.doi.org/10.1088/1751-8121/aa6dc3>.
- [CLT22] Ignacio Cirac, Sirui Lu, and Rahul Trivedi. *Lecture Note of QST Theory: Quantum Information, Winter Semester 2021/22*. Apr. 2022.
- [Pre98] John Preskill. *Lecture Notes for Physics 229: Quantum Information and Computation*. Sept. 1998.
- [Sch96] Benjamin Schumacher. *Sending quantum entanglement through noisy channels*. 1996. arXiv: [quant-ph/9604023](https://arxiv.org/abs/quant-ph/9604023) [[quant-ph](#)].
- [NC10] M.A. Nielsen and I.L. Chuang. *Quantum Computation and Quantum Information: 10th Anniversary Edition*. Cambridge University Press, 2010. ISBN: 9781107002173. URL: <https://books.google.de/books?id=j2ULnwEACAAJ>.
- [Wan23] Yuchen Wang. “QUANTUM COMPUTATION IN QUDIT SPACE AND APPLICATIONS IN OPEN QUANTUM DYNAMICS”. in: (Apr. 2023). DOI: [10.25394/PGS](https://doi.org/10.25394/PGS).

22589098.v1. URL: [https://hammer.purdue.edu/articles/thesis/QUANTUM\\_COMPUTATION\\_IN\\_QUDIT\\_SPACE\\_AND\\_APPLICATIONS\\_IN\\_OPEN\\_QUANTUM\\_DYNAMICS/22589098](https://hammer.purdue.edu/articles/thesis/QUANTUM_COMPUTATION_IN_QUDIT_SPACE_AND_APPLICATIONS_IN_OPEN_QUANTUM_DYNAMICS/22589098).



---

## List of Figures

---

1.1 Rank-r tensor in TNN with input indices $i_1, \dots, i_k$ and output indices $i'_1, \dots, i'_{k'}$ . . .	2
1.2 Binary tensor product of the tensors R and R' in TNN . . . . .	3
1.3 Partial trace over the indices $i_x$ and $i'_y$ of a tensor in TNN . . . . .	3
1.4 Grouping of the input and output indices of a tensor in TNN . . . . .	3
1.5 Singular value decomposition of a tensor in TNN . . . . .	4
2.1 Kraus representation of a quantum channel in the folded picture . . . . .	8
2.2 Trivial Kraus representation for unitary dynamics in the unfolded picture . . . . .	9
2.3 Graphical derivation of the Stinespring Dilation of a quantum channel . . . . .	9
2.4 Representation of a generic many-body quantum state in TNN . . . . .	11
2.5 First grouping step in the construction of MPS from successive SVDs . . . . .	11
2.6 Representation of a Matrix Product State in TNN . . . . .	11
2.7 Matrix Product State with translational invariance in TNN . . . . .	12
2.8 Matrix Product Density Operator in the folded picture . . . . .	12
2.9 Infinite temperature state of a quantum many-body system with L qudits . . . . .	12
2.10 Reduction of a global unitary operation to locally acting unitary gates . . . . .	13
2.11 Computation of quantum circuits . . . . .	14
2.12 Inefficient bubbling of a tensor network (sample size $L = 3$ ) . . . . .	14
2.13 Efficient bubbling of a tensor network (sample size $L = 3$ ) . . . . .	14
2.14 Contraction of the two-dimensional grid (sample size $L = 5$ ) . . . . .	15
3.1 IRF-gate in controlled unitary gate and face representation . . . . .	17
3.2 IRF-circuit in controlled unitary gate and face representation . . . . .	18
3.3 Time unitarity conditions of IRF-gates . . . . .	18
3.4 Time unitarity conditions of IRF-gates in the folded picture . . . . .	19
3.5 Dual IRF-gate in controlled gate and face representation . . . . .	19
3.6 Space-wise unitarity condition of dual IRF-gate . . . . .	19

3.7	Space unitarity conditions of Dual IRF-gates in the folded picture . . . . .	20
3.8	Unitarity conditions of the DUIRF-gate in the folded picture . . . . .	20
3.9	Computation of spatio-temporal correlation functions in TNN . . . . .	22
3.10	Correlation maps of the light cone correlators . . . . .	23
3.11	Computation of spatial correlation functions after a quantum quench . . . . .	24
3.12	Definition of solvability conditions . . . . .	24
3.13	Reduced spatial correlation function after a quantum quench . . . . .	25
4.1	Representation of an IRF-gate in the vectorised picture . . . . .	27
4.2	Definition of IRF channels in the folded picture representation . . . . .	27
4.3	Solvability conditions of IRF channels in the folded picture . . . . .	28
4.4	Graphical computation of the coefficients in the minimal example . . . . .	31
4.5	Scenario III (left) and IV (right): Application of the left (right) unitality condition	32
4.6	Completely Depolarising Channel in the folded picture . . . . .	32
4.7	Unflipped states for 3- and 4-way unital quantum channels . . . . .	33
4.8	$a = \xi = 0$ and $\nu = 1$ : Flipped states of 3-way unital quantum channels . . . . .	33
4.9	$a = \nu = 0$ and $\xi = 1$ : Flipped states of 3-way unital quantum channels . . . . .	34
4.10	$a = 1$ and $\xi = \nu = 0$ : Flipped states of 4-way unital quantum channels . . . . .	34
4.11	Identification with Controlled NOT gates of 3- and 4-way unital IRF-channels .	34
4.12	Characterisation of the middle tensor of 3- and 4-way unital IRF-channels . . .	35
4.13	Computation of spatio-temporal correlation functions of IRF channel circuits . .	36
4.14	Reduced circuits for left or right unital IRF channels . . . . .	36
A.1	Purification of a density operator in TNN . . . . .	42
A.2	Partial trace of a purified quantum state in TNN . . . . .	42

---

## Acknowledgement

---

First of all, I would like to thank Prof. Dr. Ignacio Cirac for offering me the excellent opportunity to carry out my Bachelor project in the theory division of the Max Planck Institute of Quantum Optics. I am genuinely grateful for the inspiring and supporting working environment which I could experience in the last months.

Moreover, I want to express my sincere appreciation to Prof. Dr. Jan von Delft for accepting to be my internal supervisor at the Ludwig Maximilian University of Munich. Having pursued his lecture on mathematical methods for theoretical physics in my undergraduate studies, he sparked my interest to explore physical theories with mathematical rigor. I am deeply impressed by his commitment to teaching and the ability to give his students a sympathetic hearing.

Finally, it was a great pleasure to have Dr. Georgios Styliaris guide me through my Bachelor project. When ever asked him a question, he knew to answer it precisely, conveying his deep fascination for his field of research. It cannot be taken for granted to have a supervisor spend such a considerable amount of time and dedication into this project. I am very grateful for his company in this rewarding chapter of my early scientific career.



---

## Declaration of authorship

---

I hereby declare that I have written this thesis independently and have not used any sources or aids other than those specified in this thesis.

Munich, the 1st of February 2024

A handwritten signature in black ink, appearing to read 'Matthias Pawlik', written in a cursive style.

Matthias Pawlik